République **A**lgérienne **D**émocratique et **P**opulaire
Ministère de l'**E**nseignement **S**upérieur et de la **R**echerche **S**cientifique

Université 20 août 1955-Skikda
Faculté des Sciences
Département de Physique

N° :191934036825

Mémoire de Master

Filière : Physique
Spécialité : Physique des Rayonnements

Thème

Study of the photo-electrochemical properties of Fe_2O_3-TiO_2 Nanotubes

Présenté par : **Hend HAMDANE**

Soutenu le:30/06/2025 devant le jury composé de:

A.CHETTAH	Pr	Université de Skikda	Président
N.SOBTI	MCA	Université de Batna 2	Rapporteur
S.CHAGUETMI	Pr	Université de Skikda	Co- Rapporteur
S. LABIOD	MCA	Université de Skikda	Examinateur

Année Universitaire : 2024/2025

Acknowledgments

*First, I would like to thank **Allah Almighty** for the will and patience He has granted me throughout these years of study.*

*I would also like to express my heartfelt gratitude to my **mother and father**, who have always supported me unconditionally, and to my **siblings**, with whom I shared the joys and challenges of growing up under the same roof.*

*My sincere thanks go to **Dr. Nadjah Sobti**, lecturer at the University of Batna 2, and **Dr. Samiha Chaguetmi**, professor at the University of Skikda, who kindly agreed to supervise me. Their advice and guidance were invaluable in enriching and completing this modest research work.*

*I am also grateful to the **jury members**, **Dr. A. Chettah** professor at the University of Skikda, and **Dr. S. Labiod**, lecturer at the University of Skikda, for accepting to read and evaluate my work.*

My thanks also go to all the professors of the Department of Physics and the Faculty of Science in general.

Finally, I thank everyone who helped me, directly or indirectly, in the accomplishment of this work.

Dedication

Praise be to Allah, by whose grace good deeds are completed, and through whose guidance dreams are fulfilled.

To the one whose prayers were the secret of my peace, whose smile was my comfort, and whose love has been my greatest support...

To my beloved mother, the purest heart and the most sincere love.

To the one who raised me with values, taught me dignity, and inspired me with his wisdom and calmness...

To my dear father, the pride of my life.

To my siblings, who have been my joy, my warmth, and my unwavering support.

To myself, who endured despite the hardships, stood firm through the storms, and believed that Allah never wastes the effort of those who strive.

I dedicate this humble work to everyone who supported me with a word, a prayer, a smile, or even a silent gesture of love.

And to everyone who sees knowledge as a path to elevation, and ambition as a flame that must never die.

List of Abbreviations

AC: Alternating **C**urrent

CBD: Chemical **B**ath **D**eposition

CB: Conduction **B**and

CCD: Charge-**C**oupled **D**evice

CE: Counter **E**lectrode

CPM: Counts **P**er **M**inute Detector

DRS: Diffuse **R**eflectance **S**pectroscopy

EIS: Electrochemical **I**mpedance

Eg: Band **G**ap **E**nergy

FEG: Field **E**mission **G**un

IR: Infrared

MEB: Scanning **E**lectron **M**icroscope

NPs: Nano**p**article**s**

NTs: Nano**t**ube**s**

PC: Photo**c**urrent

PEC: Photo**e**lectro**c**hemical

PTFE: Poly**t**etra**f**luoro**e**thylene

RE: Reference **E**lectrode

SEM: Scanning **E**lectron **M**icroscope

UV: Ultra**v**iolet

VB: Valence **B**and

VIS: Visible **S**pectrum

WE: Working **E**lectrode

XRD: X-ray **D**iffraction

Table of contents

General Introduction 1

Chapter I:A literature review on TiO_2, Fe_2O_3 and water-splitting photoelectrolysis

I.Introduction 3

I.1.Fundamentals of Photoelectrochemical Water Splitting 3

I.1.1.Principle and Definition 3

I.1.2.Process Description 4

I.2.Photoelectrochemical Cell 5

I.2.1.Photoelectrochemistry, Semiconductor/Electrolyte Interface 5

I.2.1.1.Definition 5

I.2.1.2.Semiconductor-Electrolyte Interface 6

I.2.1.3.Selection of Electrodes for the PEC Systems 7

I.2.1.4.Semiconductor behavior under illumination 8

I.2.1.5. Semiconductor electrode immersed in an electrolyte 9

I.2.1.6. Effects of semiconductor type on PEC response 11

I.3. Hydrogen production 12

I.4.Properties of titanium dioxide 13

I.4.1.Crystallineproperties 13

I.4.2.Electronic properties 14

I.4.3.Optical properties 14

I.5. Nanostructured TiO_2 14

I.6. Anodization method 15

I.7. Chemical bath deposition (CBD) 16

I.8. Iron oxide 16

I.8.1.Crystalline structure 16

I.8.2. Optical properties 17

I.9. Fe_2O_3-TiO_2hetero-nanostructures 17

I.10.Application of Fe_2O_3-TiO_2nanotubes (NTs) 18

I.11. Conclusion 19

Chapter II:**Samples elaboration and characterization**

II.Introduction 20

II.1.Synthesis of Fe_2O_3-TiO_2 Nanotubes 20

II.1.1. Materials and Chemicals 20

II.1.2.Fabrication of Self-Organized Crystalline TiO_2 Nanotubes 21
II.1.2.1. Surface Preparation 21
II.1.2.2.ElectrolytePreparation 21
II.1.2.3.Anodization Process 22
II.1.2.4.Post-Treatment 22
II.1.3. Preparation of Fe_2O_3-TiO_2Nanotubes 24
II.2.Characterization techniques for Fe_2O_3- TiO_2Nanotubes 25
II.2.1. X-ray Diffraction (XRD)analysis 25
II.2.2.Raman spectroscopy 27
II.2.3.UV-Vis Diffuse Reflectance Spectroscopy (DRS) 28
II.2.5.Photoelectrochemical (PEC)characterization 31
II.3.Conclusion 34

Chapter III: **Results and discussion**

III. Introduction 35
III.1.X-ray Diffraction analysis 35
III.2.Raman spectroscopy analysis 36
III.3.SEM analysis 37
III.4.UV-Vis DRS analysis 38
III.5.Photoelectrochemical properties of Fe_2O_3-TiO_2 NTs 40
III.5.1.Comparison of PEC properties between TiO_2 and Fe_2O_3-TiO_2 NTs 40
III.5.2.Photocurrent performance of TiO_2 and Fe_2O_3–TiO_2 NTs (On/Off Cycles) 42
III.6.Electrochemical impedance spectroscopy (EIS) analysis of TiO_2 and Fe_2O_3-TiO_2NTs .. 43
III.7. Conclusion 44
General Conclusion 46
References: 47

List of Figures

Chapter I

Figure I.1: Schematic representation of the photoelectrolysis process……..…. 5
Figure I.2: Schematic diagram of a photoelectrochemical cell…….. 6
Figure I.3: Electron-hole pair generation in (a) n-type and (b) p-type semiconduc-tors, showing the effects on quasi-Fermi levels and charge carrier densities……..…. 8
Figure I.4: (a) Distribution of the energy states of a redox couple in solution and representation of the energy diagram of a p-type semiconductor. (b-c) Current-voltage characteristics (i-V curves) for semiconductor/electrolyte junctions in dark conditions: (b) n-type and (c) p-type semiconductors…… 10
Figure I.5: Current-voltage response of an illuminated semiconductor-electrolyte interface. Red: majority carrier contribution (identical in dark and light). Blue: photogenerated minority carrier current……...… 11
Figure I.6: Current-voltage characteristics under alternating illumination for n-type (a) and p-type (b) semiconductor/electrolyte interfaces……... 12
Figure I.7: Structural polymorphs of TiO_2: (a) rutile, (b) brookite, (c) anatase……. 13
Figure I.8: Optical interference colors generated on titanium through electrochemical anodization, showing the voltage-dependent color spectrum…….. 15
Figure I.9: Crystallographic structure of α-Fe_2O_3 (red = oxygen, brown = iron)…….... 16

Chapter II

Figure II.1: Polishing using silicon carbide……..... 21
Figure II.2: Anodization Process……..... 22
Figure II.3: Post-anodization processing of TiO_2 NTs: (a) rinsing step; (b) thermal crystallization at 450°C……..... 23
Figure II.4: Cyclic Deposition…….……... 24
Figure II.5: Principle of X-ray diffraction by a Crystal and illustration of Bragg's Law…….….. 26
Figure II.6: Panalytical Empyrean Diffractometer…….…..... 26
Figure II.7: Example of three different scattering mechanisms showing a given input wavelength compared with scattered wavelengths …….....… 27

Figure II.8: Schematic of Raman spectroscopy instrumentation……...… 28
Figure II.9: Jasco ILN-725-V-676 diffuse reflectance spectrophotometer…… 29
Figure II.10: JEOL JSM-7600 microscope……..….. 31
Figure II.11: Potentiostat Experimental Setup……..... 33

Chapter III

Figure III.1: XRD patterns of TiO_2 NTs arrays, (a) as-prepared amorphous TiO_2 NTs, (b) crystalline TiO_2 NTs after annealing at 450 °C for 1 hour, and (c) Fe_2O_3-modified TiO_2prepared via the impregnation method and annealed at 550°C…… 35
Figure III.2: Raman spectra of (a) bare TiO_2 NTs arrays and (b) Fe_2O_3- modifiedTiO_2 NTs prepared via CBD method……..….... 37
Figure III.3: Scanning electron microscopy (SEM) images showing: (a) top-view of as-prepared TiO_2 nanotube arrays, (b) Fe_2O_3-modified TiO_2 NTs prepared via impregnation, and (c) corresponding energy-dispersive X-ray spectroscopy (EDX) analysis of the Fe_2O_3-TiO_2 NTs……..... 38
Figure III.4:UV-Vis diffuse reflectance spectra of (a) TiO_2 nanotubes arrays and (b) Fe_2O_3-modified TiO_2 NTs prepared via CBD method with subsequent annealing at 550°C……...……. 39
Figure III. 5(a): Determination of the band gap of TiO_2 NTs, and of Fe_2O_3-TiO_2 NTs……..... 40
Figure III.6: Current–potential characteristics in 1 M NaOH solution for bare TiO_2 NTs array in the dark (a) and under simulated solar light (b), and for Fe_2O_3-TiO_2 NTs under simulated solar light (c)…….…….. 41
Figure III.7: Transient photocurrent response under chopped illumination at 0V vs.Ag/AgCl for pristine TiO_2 NTs (a) and Fe_2O_3-TiO_2 NTs samples (b) in a 1 M NaOH electrolyte……... 43
FigureIII.8: Nyquist plots of TiO_2 NTs and Fe_2O_3-TiO_2 NTs electrodes recorded in 1M NaOH…….. 44

List of Tables

Table II.1: Chemical reagents and materials employed in the fabrication of Fe_2O_3-TiO_2 NTs…….….. 20

Table II.2: Chemical reactions during TiO_2 nanotube formation via anodization and crystallization…… 23

Table II.3: Chemical reaction mechanism for hematite (Fe_2O_3) deposition on anodized TiO_2 nanotubes…….. 25

General Introduction

General Introduction

The field of materials science is undergoing rapid advancements, particularly in the development and engineering of nanostructured materials. Precise control over material nanostructures has become a key research focus, as it critically determines their physical, chemical, and electronic propertiesof materials. Among various nanostructures, those designed for energy, environmental, and photocatalytic applications have attracted significant attention due to their transformative potential across multiple disciplines. Addressing global energy challenges requires not only meeting escalating energy demands but also minimizing environmental impacts, particularly greenhouse gas emissions.

Renewable energy sources like solar and wind, though clean and abundant, face challenges of intermittency. In this context, hydrogen-based technologies are emerging as a particularly promising solution for clean and sustainable energy systems.However, the industrial-scale hydrogen production, storage, and utilization present significant scientific and technological challenges. As an energy carrier rather than a primary energy source, hydrogen (H_2) requires production through various methods. Currently, fossil fuel-based processes, particularly steam methane reforming and coal gasification, dominate hydrogen production.

Alternative approaches include biomass conversion and water splitting, with the latter being especially attractive due to its potential for clean, renewable hydrogen generation. Among these, water splitting techniques encompass electrolysis, thermo-chemical and photochemical processes, and bio-photolysis. While electrolysis represents the most developed technology, it frequently relies on electricity generated from non-renewable sources.Consequently, solar-driven water splitting via photocatalysis or photoelectrochemical (PEC) processes represents a crucial scientific objective. This field gained momentum following the groundbreakingwork of Fujishima and Honda (1972), who first demonstrated photoelectrochemical water splitting using TiO_2 electrodes under UV illumination. Their pioneering study established titanium dioxide as a material of significant interest in this domain.

TiO_2 is an extensively studied n-type semiconductor, and it exhibits exceptional photocatalytic activity, remarkable chemical stability, and excellent environmental compatibility. However, its practical efficiency under solar irradiation is constrained by a

wide band gap that limits light absorption to the ultraviolet spectrum. To overcome this limitation, significant research efforts have focused on modifying TiO_2 through heterojunction formation with narrow-bandgap semiconductors such as iron oxide (Fe_2O_3, hematite). With its narrower bandgap (~2.1 eV) and visible light absorption capability, Fe_2O_3presents an ideal complement to TiO_2-based systems. The strategic integration of Fe_2O_3 with TiO_2 nanostructures is anticipated to achieve three synergistic effects: improved charge carrier separation, extended light absorption into the visible spectrum, and enhanced overall efficiency in both photocatalytic and photoelectrochemical processes.

In this study, TiO_2 nanotubes arefabricated via anodization, an efficient electrochemical technique that produces highly ordered tubular structures with large surface areas, making them ideal for photoelectrochemical applications. Subsequently, Fe_2O_3 nanoparticles are deposited onto the TiO_2 nanotubes using chemical bath deposition (CBD), followed by thermal treatment. This composite architecture isdesigned to leverage the synergistic effects of both semiconductors, enhancing photoelectrochemical performance under visible light.

The primary objective of this research is to investigate the influence of Fe_2O_3 modification on the structural, optical, and photoelectrochemical propertiesof TiO_2 nanotubes. The findings areexpected to providevaluable insights for designing advanced photocatalytic materials for hydrogen production, with broader implications in environmental science, chemistry, physics, and nanotechnology.

This thesis is organized into three chapters:

- **Chapter One** provides a comprehensive literature review on TiO_2 and Fe_2O_3 semiconductors, covering their structural, optical, and electronic properties, as well as the fundamental principles of photoelectrochemical water splitting.
- **Chapter Two** describes the synthesis methodsemployed to fabricate the nanostructured materials, particularly anodization and chemical bathdeposition, and details the techniques used for their physico-chemical characterization.
- **Chapter Three** presents and analyzes the experimental results, focusing on the materials' photoelectrochemical performance and their potential for hydrogen production through water splitting. The thesis concludes by summarizing the key findings and proposing directions for future research.

CHAPTER I

A literature review on TiO_2, Fe_2O_3 and water-splitting photoelectrolysis

This chapter provides a comprehensive literature review focusing on hydrogen production via water splittingtechnologies and the fundamental properties of titanium dioxide (TiO_2), iron oxide (Fe_2O_3), and Fe_2O_3-TiO_2 heterostructures. The discussion encompasses their crystallographic structures and optical characteristics. The chapter concludes with an overview of current applications for both TiO_2 and Fe_2O_3-modified TiO_2 nanotube systems.

I. Introduction

The global transition toward sustainable energy systems necessitates the development of efficient and environmentally benign technologies for clean fuel production. In this context, hydrogen production via water photoelectrolysis, also known as photoelectrochemical (PEC) water splitting, has emerged as a particularly promising approach, enabling direct conversion of solar energy into chemical energy through the dissociation of water molecules using semiconductor photoelectrodes. Among the various materials investigated for this application, titanium dioxide (TiO_2)andhematite (Fe_2O_3)have received significant scientific interest. TiO_2 is well-known for its exceptional chemical stability, non-toxicity, and natural abundance, establishing it as a benchmark photo-anode material. However, its practical implementation is constrained by a wide bandgap (~3.2 eV), restricting light absorption to the ultraviolet spectrum. Conversely, hematite possesses a more favorable narrow bandgap (~2.1 eV) for visible light harvesting, yet its performance is limited by poor charge carrier mobility (~0.1cm^2 $V^{-1}s^{-1}$) and rapid electron-hole recombination. This review systematically examines the fundamental properties of photoelectrochemical performance, and recent optimization strategies for TiO_2 and Fe_2O_3-based photoelectrodes, with particular emphasis on their application in solar water splitting systems.

I.1. Fundamentals of Photoelectrochemical Water Splitting

Photoelectrochemical (PEC) water splitting is a process that converts solar energy into chemical energy by using light to drive the decomposition of water into hydrogen (H_2) and oxygen (O_2). This reaction is carried out in a photoelectrochemical cell, which typically consists of a photoanode, a cathode, and an electrolyte.

I.1.1. Principle and Definition

Photoelectrolysis is a solar-driven electrochemical process that dissociates water molecules through the combined action of photon energy and applied electrical potential. This dual energy input enables the conversion of solar and electrical energy into storable chemical energy. The solar energy conversion is mediated by semiconductor materials that functionas photocatalysts[1],absorbing incident photons to generate electron-hole pairs. These photoactive semiconductors, when employed as electrodes immersed in an aqueous

electrolyte, constitute photoelectrochemical (PEC) cells. Conceptually, PEC systems can be viewed as integrated photovoltaic-electrolyzer devices where light absorption and water electrolysis occur in a single unit operation. Despite their apparent simplicity in principle, the development of efficient PEC systems for practical hydrogen production remains in the early stages of fundamental research, with significant challenges persisting in both materials science and device engineering.

Four main steps are involved in the photoelectrochemical process of water dissociation:

- **The first step:** consists of the generation of an electronic charge at the surface of the photo-anode subjected to solar radiation, producing electron-hole pairs.

- **The second step:** is the oxidation of water at the photo-anode by holes, producing oxygen molecules.

- **The third step:** is that of the transport of hydrogen ions and electrons from the photo-anode to the cathode, respectively via the electrolyte and the electrical connection (the cathode potentially being a light-induced photocathode).

- **The fourth step:** represents the reduction step of H^+ ions at the cathode into hydrogen (H_2) molecules with the help of electrons [2, 3].

I.1.2. Process Description

An applied electric current induces water dissociation ($H_2O \rightarrow H^+ + OH^-$) in the electrolytic cell. At the cathode, hydrogen ions (H^+) undergo reduction by accepting electrons, producing gaseous hydrogen (H_2) through the following half-reaction [1]:

$$2H^+ + 2e^- \rightarrow H_2 \qquad (I.1)$$

While the oxidation of hydroxide ions, which lose electrons, occurs at the anode to "close" the electrical circuit (balancing the chemical reaction in terms of charges):

$$2H_2O \rightarrow O_2 + 4H^+ + 4e^- \qquad (I.2)$$

This gives the following electrolysis decomposition equation:

$$2H_2O \rightarrow 2H_2 + O_2 \qquad (I.3)$$

The amount of gaseous dihydrogen produced is thus twice that of dioxygen (Figure I.1). According to Avogadro's law, the volume of dihydrogen produced is also twice as large as that of dioxygen [3].

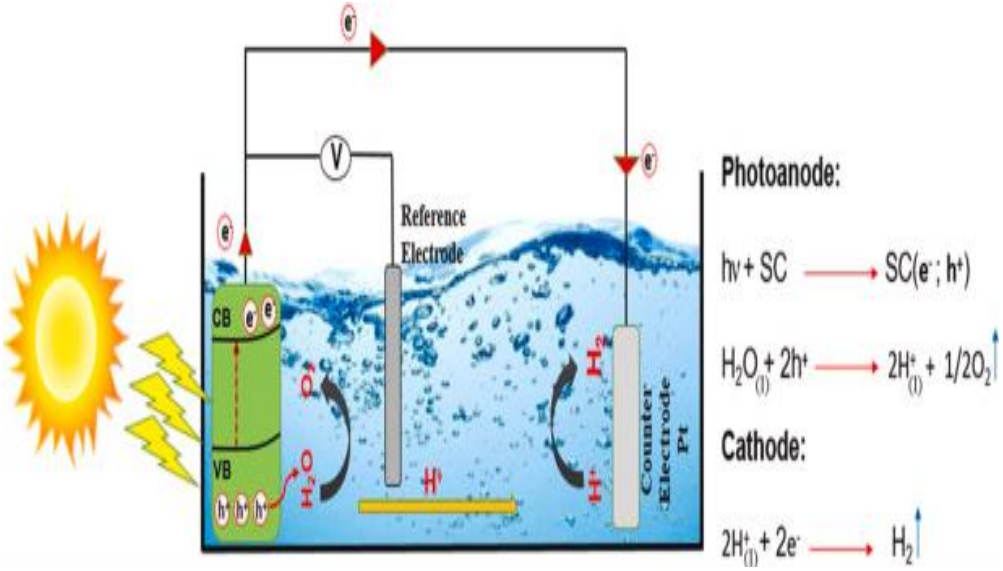

Figure I.1: Schematic representation of the photoelectrolysis process [3].

I.2. Photoelectrochemical Cell

I.2.1. Photoelectrochemistry, Semiconductor/Electrolyte Interface

I.2.1.1.Definition

Photoelectrochemistry is the branch of chemistry that investigateselectron transferprocesses influenced by light irradiation on a material.According to Honda[4], photoelectrochemistryencompasses the reactions taking place on an electrode in an excited state. This excitation may involve:

- The metallic or semiconducting electrode itself,
- Molecules adsorbed on the electrode surface.
- Species at the electrode/electrolyte interface.

These reactions can also result from the excitation of reactive compounds in solution. Photoelectrochemistry primarily focuses on semiconductor materials and serves as a powerful tool for assessing the photoactivity (or activity under irradiation) of crystalline and nanocrystalline semiconductors, such as TiO_2[5]. Titanium dioxide (TiO_2) is the most extensivelystudied photoelectrode material and was first successfully demonstrated in

photoelectrochemical (PEC) cells by Honda and Fujishima in the 1970s. Since then, research has expanded to include other semiconductor materials, notably zinc oxide (ZnO) and tungsten trioxide (WO_3). Broadly, photoelectrochemistry examines the influence of light irradiation on charge transfer processes at the semiconductor/electrolyte interface [5]. A photoelectrochemical reaction thus encompasses all phenomena that convert photon energy into electrical energy (via electron-hole pair generation), subsequently driving chemical reactions such as oxidation and reduction processes (Figure I.2).

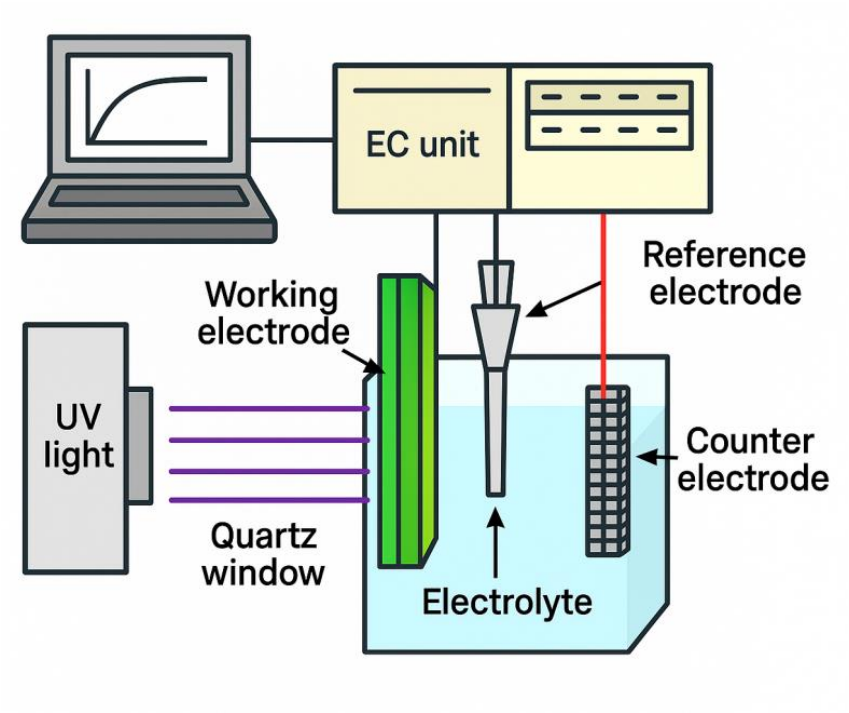

Figure I.2: Schematic diagram of a photoelectrochemical cell.

I.2.1.2.Semiconductor-Electrolyte Interface

A semiconductor is a material with electrical conductivity intermediate between insulators and metals. Its electronic structure consists of a filled valence band (VB) and an empty conduction band (CB), separated by a band gapE_g. For an electron to contribute to electrical conduction, it must acquire sufficient external energy to transition from the valence band to the conduction band. This energy can besupplied either thermally (kT) or electromagnetically (hν). When an electron is excited into the conduction band, it leaves behind a positively charged vacancy in the valence band, known as a hole (h^+)[1, 6].This processgenerates electron-hole pairs (e^-, h^+).Under an applied electric field, electrons in the

conduction band migrate toward regions of higher potential, while holes in the valence band effectively move in the opposite direction.This occurs as electrons successively fill vacant sites, creating the illusion of hole movement.Titanium oxide (TiO_2) is intrinsically a n-type semiconductor due to its higher concentration of negative charge carriers (electrons) compared to positive charge carriers (holes). If n_i represents the intrinsic carrier density (equal for both electrons and holes in an undoped semiconductor), the Maxwell-Boltzmann approximation yields:

$$n \times p = n_i^2 \qquad \text{(I.4)}$$

Where:

$$n = N_c \exp\left(-\frac{E_c - E_f}{k_B T}\right) \qquad \text{(I.5)}$$

$$p = N_v \exp\left(-\frac{E_f - E_v}{k_B T}\right) \qquad \text{(I.6)}$$

Here:

N_c and N_v are the density of states in the conduction band (CB) and valence band (VB), respectively.

k_B is the Boltzmann constant.

$E_f$is the Fermi level, defined as the reference electrochemical potential for electron occupation in energy levels.

At equilibrium (no applied voltage or carrier injection), the Fermi level remains constant, representing a uniform electrochemical potential for electrons throughout the material [1, 7].

I.2.1.3.Selection of Electrodes for the PEC Systems

Electrodesserve asthe active sitesfor electrochemical reactions in photoelectrochemical (PEC). They typically consist of:

- A catalytic material layer (where redox reactions occur),
- A diffusion layer (which enhances current flow and facilitates the transport of reactants and products) [8].

When selecting semiconductor materials for PEC applications, two critical criteria mustbe considered:

a. The presence of an *optimal bandgap*.

b. The ability to minimize charge carrier recombination.

For watersplitting applications, the photoanode must absorb photons with a minimum energy of 1.23 eV (the theoretical electromotive force required to dissociate water molecules) [6].

I.2.1.4.Semiconductor behavior under illumination

When a semiconductor absorbs photons with energy exceeding its band gap E_g, electron-hole pairs are generated. The separation of these charge carriers leads to:

- Increased free electron concentration in the conduction band.
- Increased hole concentration in the valence band.

Observations regarding charge carrier dynamics:

a. Majority carriers experience a modest increase in density due to their already high concentration.

b. Minority carriers show a significant increase compared to their dark-state concentration.

This phenomenon is illustrated schematically in Figure I.3[1, 9].

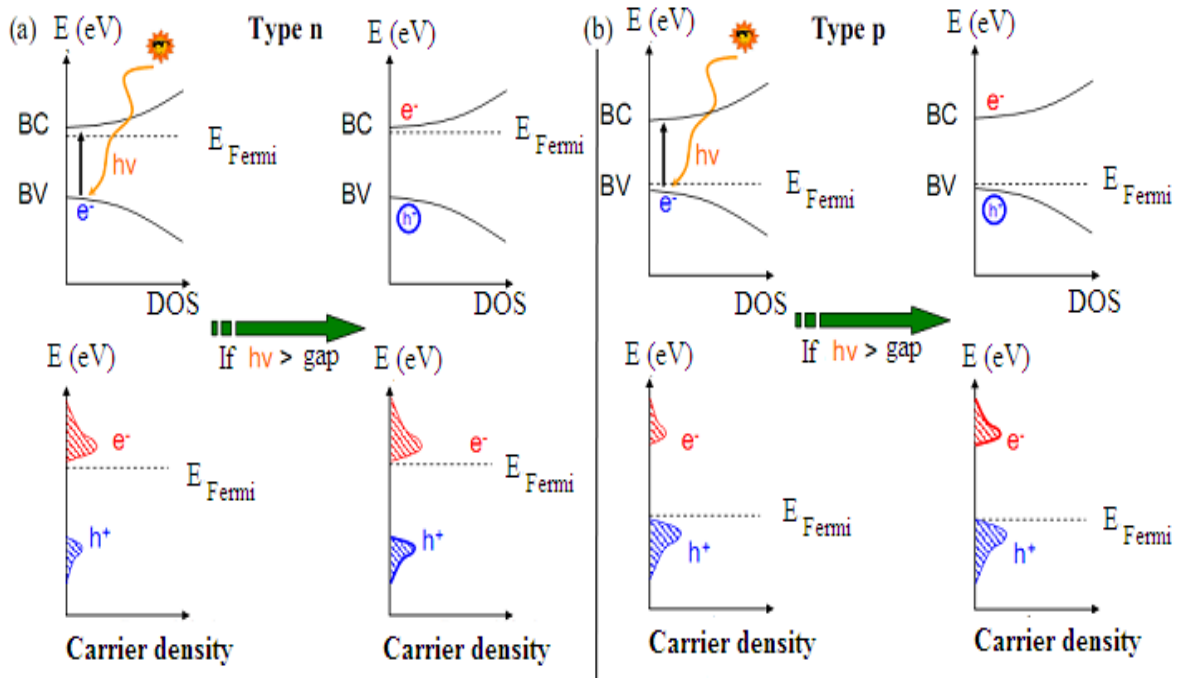

Figure I.3: Electron-hole pair generation in (a) n-type and (b) p-type semiconductors, showing the effects on quasi-Fermi levels and charge carrier densities.

I.2.1.5. Semiconductor electrode immersed in an electrolyte

This section examines the case where a semiconductor electrode replaces one of the metallic electrodes in an electrochemical system. The phenomena occur at the semiconductor-electrolyte interface:

a. Fermi level alignment

When the semiconductor contacts the electrolyte, their Fermi levels equilibrate at the interface. The semiconductor's Fermi level adjusts to match the solution potential established by the electrochemical apparatus [1, 9].

b. Redox species distribution

The distribution of oxidized/reduced species in solution follows a probability function around the reaction potential, analogous to the Fermi-Dirac distribution (Figure I.4a). The applied potential determines whether oxidized or reduced species dominate, enabling electrochemical reactions through charge transfer across the interface.

c. Interface characteristics

FigureI.4a schematically shows a p-type semiconductor in depletion mode the typical operational state for semiconductor electrodes. In this configuration:

- Band bending drives majority carriers toward the bulk.
- Minority carriers accumulate near the surface.

d. Water Electrolysis and Current Limitations

While semiconductor electrodes enable water electrolysis through their charge carriers, minority carrier limitations create distinct behavior:

- **n-type:** Oxidation current reaches a plateau.
- **P-type:** Reduction current reaches a plateau (Figures I.4b and I.4c).

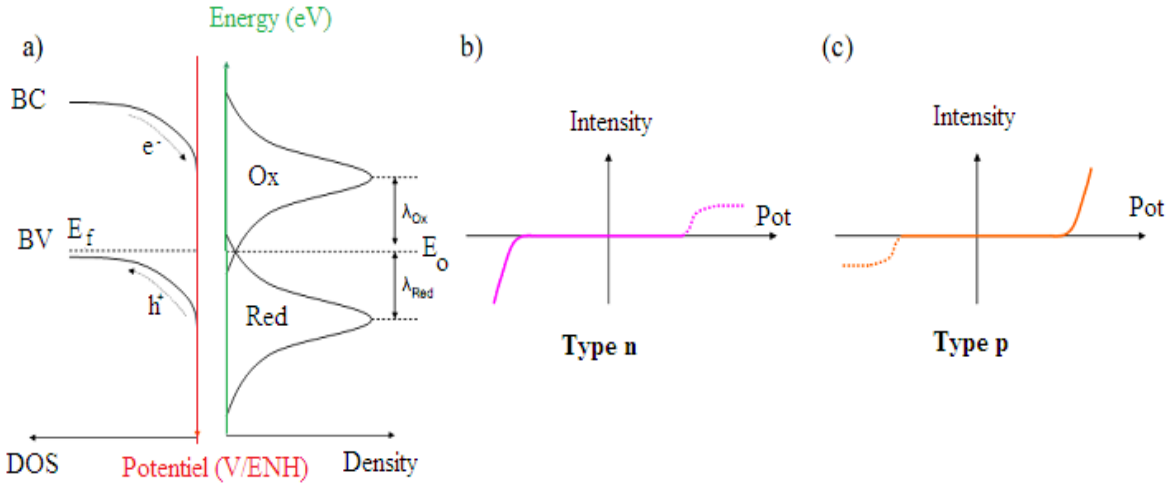

Figure I.4:(a) Distribution of the energy states of a redox couple in solution and representation of the energy diagram of a p-type semiconductor. (b-c) Current-voltage characteristics (i-V curves) for semiconductor/electrolyte junctions in dark conditions: (b) n-type and (c) p-type semiconductors [9].

e. Photoelectrochemical behavior under illumination

When illuminated, a semiconductor electrode exhibits significant changes in charge carrier dynamics:

1. Carrier generation and transport

- Photogenerated minority carriers migrate toward the semiconductor surface.
- Majority carriers move toward the bulk material.
- This separation creates both a surface photopotential and photocurrent.

2. Depletion zone effects

- In the depletion region (where dark current is minimal).
- Increased minority carrier density enables redox reactions with the electrolyte.
- Results in either:

  - Positive current contribution (n-type semiconductors).
  - Negative current contribution (p-type semiconductors) [1, 9].

3. Photocurrent characteristics

- Dependent on minority carrier transfer kinetics to electrolyte.
- Demonstrated in Figure I.5through current comparisons:
  - Dark conditions (red curves).
  - Illuminated conditions.
- Current sign differences under illumination reveal semiconductor type.
- Depletion region current analysis determines photocurrent nature (anodic/cathodic).

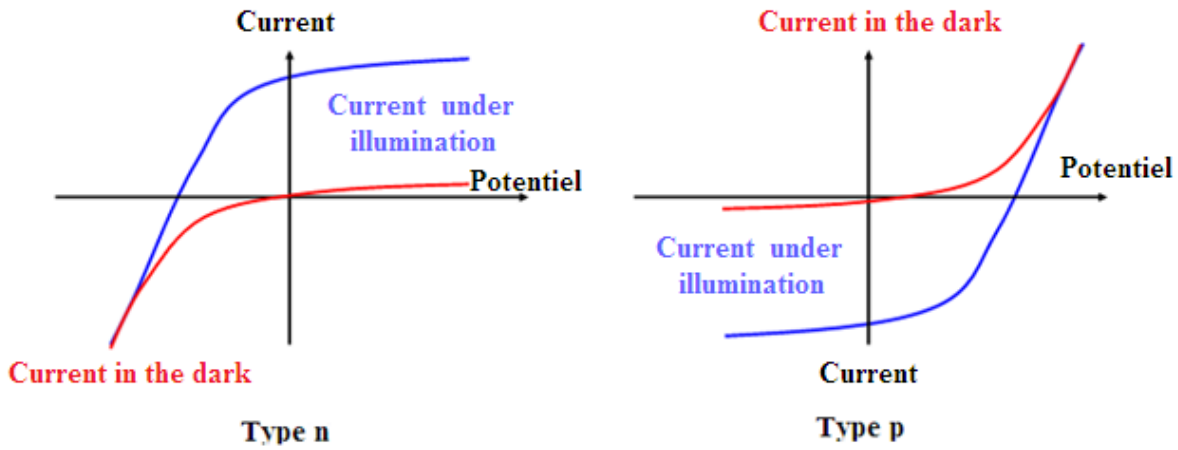

Figure I.5: Current-voltage response of an illuminated semiconductor-electrolyte interface. Red: majority carrier contribution (identical in dark and light). Blue: photogenerated minority carrier current [9].

I.2.1.6. Effects of semiconductor type on PEC response

The semiconductor type (n-type or p-type) critically determines its photoelectron-chemical (PEC) behavior. When subjected to an applied potential in an aqueous electrolyte, each type exhibits distinct characteristics:

a. Minority carrier dynamics

- Illumination within the semiconductor's depletion region (between water's oxidation and reduction potentials) generates excess minority carriers.
- This leads to measurable current variations:

- **n-type**: Current shifts toward *positive* values (anodic).
- **p-type**: Current shifts toward *negative* values (cathodic).

b. Theoretical framework

The observed current oscillations reflect the interplay between:

- Band bending in the depletion region.
- Minority carrier diffusion to the interface.

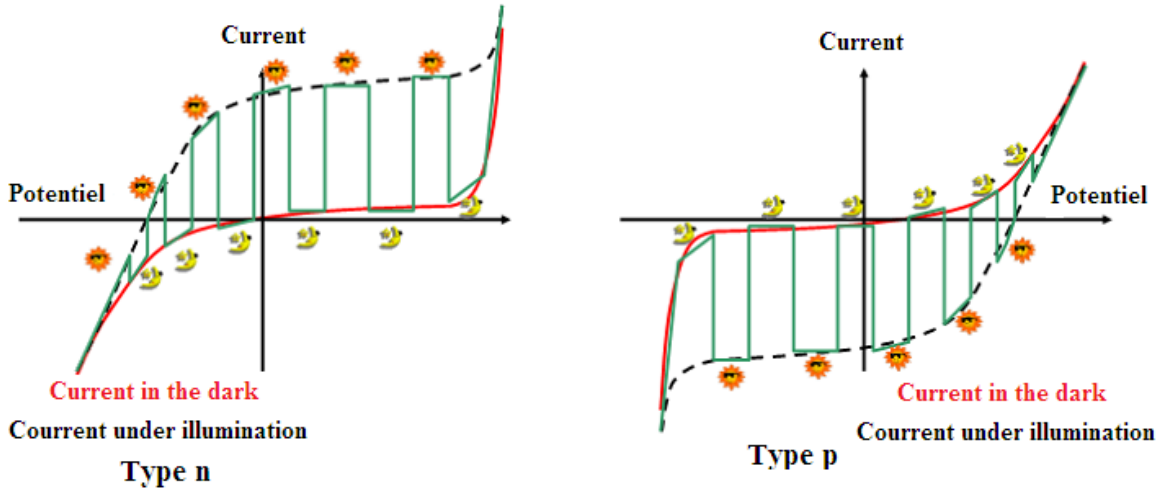

Figure I.6: Current-voltage characteristics under alternating illumination for n-type (a) and p-type (b) semiconductor/electrolyte interfaces [1].

I.3. Hydrogen production

Currently, nearly all hydrogen production derives from two primary sources:hydrocarbon decomposition and water electrolysisstandout as one of the most promising technologies for sustainable hydrogen production, offering two advantages:

a. Clean production process (zero carbon oxide emissions).
b. High-purity hydrogen output.

However, widespread adoption of electrolysis faces significant challenges due to its high operational costs. This economic barrier has spurred research into alternative energy sources

for hydrogen production, including Wind power, Hydropower, Solar energy, Geothermal energy, Biomass-based energy systems [10].

I.4. Properties of titanium dioxide

I.4.1.Crystallineproperties

TiO_2 exhibits three primary polymorphic forms (Figure I.7):

a. **Rutile** (tetragonal).
b. **Anatase** (tetragonal).
c. **Brookite** (orthorhombic).

- ***Phase Stability and Transitions***:
  - ❖ While rutile is thermodynamically stable at 0K, the energy difference between rutile and anatase is minimal (2–10 kJ/mol).
  - ❖ Anatase irreversibly transforms to rutile at 450–1200°C.

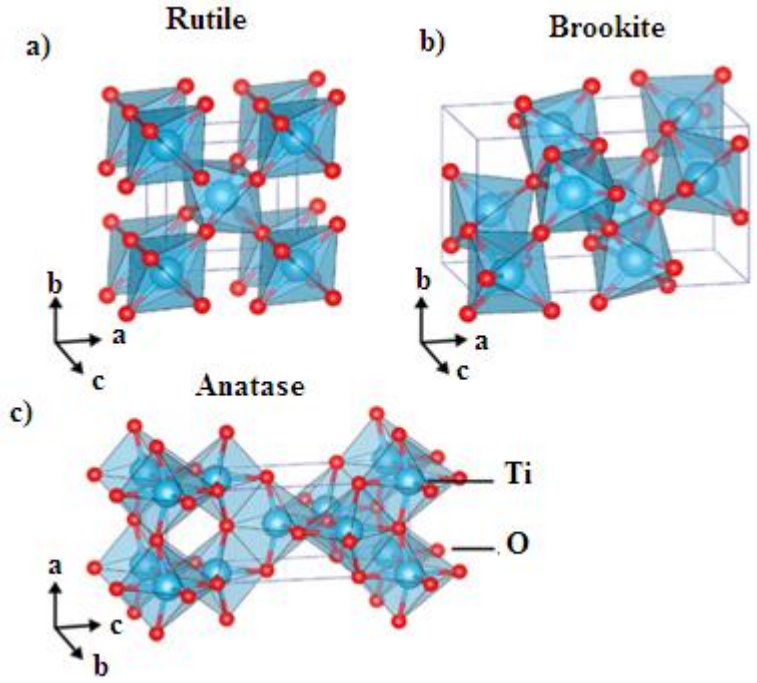

Figure I.7: Structural polymorphs of TiO_2: (a) rutile, (b) brookite, (c) anatase[11].

This transformation is temperature-dependent but also influenced by factors such as dopant concentration, initial phase, and particle size. It has also been observed that both brookite and anatase phases tend to transform into rutile at specific particle sizes, with rutile

becoming more stable than anatase when particle sizes exceed 14 nm. Additionally, when the rutile phase forms, it grows faster compared to the anatase phase [12].

I.4.2.Electronic properties

Titanium dioxide can be considered either as an n-type semiconductor with a wide bandgap or as an oxide with a narrow bandgap. It has a bandgap slightly exceeding (~3.2 eV). In its stoichiometric state, the occupied states primarily derive from oxygen atoms, while the free states originate from titanium atoms. Upon reduction, the material contains oxygen vacancies. For the three crystalline forms of TiO_2 previously mentioned, the valence band is formed by the overlap of the titanium e_g orbitals and the oxygen 2p orbitals[13,14].

I.4.3.Optical properties

TiO_2 is known for its optical properties, including its high refractive index. Among its three crystalline phases, rutile has the highest refractive index. Titanium dioxide exhibits a high coverage rate, and by combining this property with its particularly high refraction, it reflects 96% of the incident light in the visible spectrum, which gives its white color at the micrometric scale (as a powder). Due to these properties, TiO_2 is the mostopaque white pigment used in industry (paints, coatings, plastics, inks, pharmaceuticals, toothpastes, food coloring) [15].

I.5.Nanostructured TiO_2

The wide-ranging properties of titanium dioxide have generated a great deal of interest in various diverse fields. Consequently, in recent years, numerous researchers have directed their investigations toward the synthesis and processing of nanostructured titania. One of the majority obvious advantages provided by nanomaterials is that of the significantly increased surface area presented by small particles. Furthermore, the transition from macroscale to nanoscale can alter electrical properties as a result of quantum effects induced by the extremely small particle dimensions. Among the established methods for the synthesis of nanostructured titania, including nanotubes, nanowires and nanopores, the most important technique are anodization, sol-gel, hydrothermal, and vapor deposition methods[16, 17]. While a detailed discussion of these methods is beyond the scope of this work, particular emphasis is placed on the formation of nanostructured titanium dioxide via anodization in

fluoride-containing electrolytes, especially nanotubes. Anodization has involved interest as a cost-effective technique and approach for fabricating nanostructured TiO_2[18,19].

TiO_2 has unique properties that make it ideal for use in various fields. Additionally, this material is cheap and widely available, making it a cost-effective option. Furthermore, TiO_2 possesses chemical and physical stability, enhancing its value as a nanomaterial, especially in the form of nanotubes[20].

I.6.Anodization method

The anodization of metals, especially aluminum and titanium, is a well-established technique used to produce a protective oxide layer on the metal surface.Both aluminum and titanium exhibit a high affinity for oxygen, these metals, once exposed to the air, are covered by a thin layer of protective oxide few nanometers thick[19]. Researchers haveextensively studied to enhance the quality and thickness of the natural oxide layer to improve the metal's corrosion resistance, a critical factor in many industrial applications, as well as the overall quality of the surface film. By processes exploiting electrochemical processes it is possible to address and solve these problems. Anodization of titanium is normally associated with the colouring process, the result of an optical interference effect, used for the production of jewellery[19, 21]. As illustrated in Figure I.8 [15, 17], the observed colors arise solely from the optical interference caused by a thin, transparent oxide film on the metal surface, with the specific hue dependent on the applied voltage. In contrast, the native oxide layer is too thin to produce such interference effects, remaining colorless (see the left side ofFigure I.8).

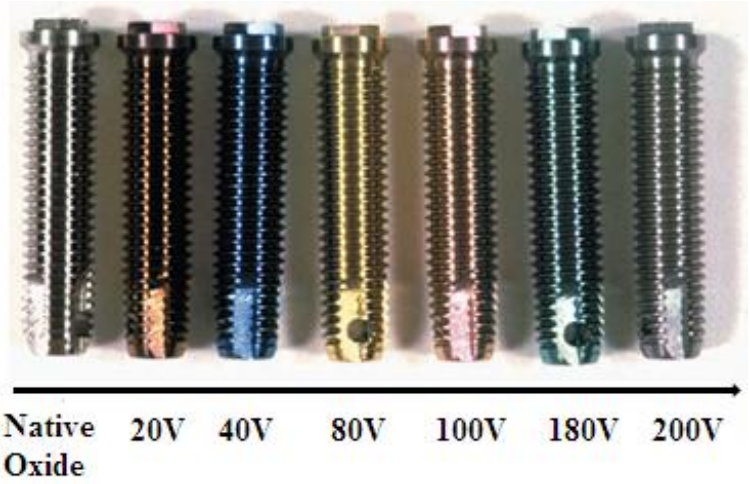

Figure I.8: Optical interference colors generated on titanium through electrochemical anodization, showing the voltage-dependent color spectrum [19].

I.7.Chemical bath deposition (CBD)

Chemical bath deposition, also called chemical solution deposition[23] and CBD, is a method of thin-film deposition (solids forming from a solution or gas), using an aqueous precursor solution [23]. Chemical bath deposition typically forms films usingheterogeneous nucleation (deposition or adsorption ofaqueous ions onto a solid substrate)[24], to form homogeneous thin films of metal chalcogenides (mostly oxides, sulfides, and selenides) [23] and many less common ionic compounds [23, 25]. CBD involves forming a solid film by controlling the precipitation of a compound onto a suitable substrate through simple immersion in a bath where all the chemical precursors are dissolved simultaneously. The thickness of the deposited layer as well as the growth rate of the films depends on easily controllable factors such as bath temperature and reactant concentration. So, chemical bath deposition produces films reliably, using a simple process with little infrastructure, at low temperature, and at low cost [23]. Furthermore, chemical bath deposition can be employed for large-area batch processing or continuous deposition. Films produced by CBD are often used in semiconductors, photovoltaic cells, and supercapacitors, and there is increasing interest in using chemical bath deposition to create nanomaterials [23, 26]. This method used for the decoration of TiO_2nanotubes with iron oxide nanoparticles(this work).

I.8.Iron oxide

I.8.1.Crystalline structure

Hematite is an iron oxide mineral (Fe_2O_3) and is the primary ore used for iron production. It is characterized by its red or brown color and has a crystal structure similar to corundum (α-Al_2O_3), but it is more reactive due to its surface, which contains types of oxygen that can absorb pollutants more efficiently.Figure I.9 illustrates the crystallographic structure of α-Fe_2O_3.

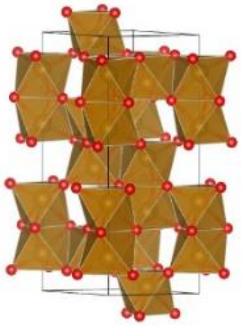

Figure I.9: Crystallographic structure of α-Fe_2O_3 (red = oxygen, brown = iron) [27].

I.8.2.Optical properties

Hematite (α-Fe_2O_3) exhibits interesting optical properties that make it a promising material for photoelectrochemical (PEC) water splitting and other optoelectronic applications. It has a relatively small band gap of approximately 2.2 eV, enabling it to absorb a significant portion of sunlight while maintaining good electrochemical stability. In comparison to titanium dioxide (TiO_2), which has a larger band gap of around 3.2 eV, hematite's narrower band gap allows for broader absorption in the visible light spectrum. Both materials are semiconductors commonly used as photocatalysts [28]. Moreover, hematite has demonstrated effective performance as a semiconductor electrode material for solar water splitting in hydrogen fuel research. Its suitable band gap, along with its non-toxicity, natural abundance, and low cost, makes it an attractive candidate for solar energy conversion applications [27].

I.9.Fe_2O_3-TiO_2hetero-nanostructures

Iron oxide is a well-known semiconductor in the literature, with a bandgap of approximately 2.2 eV, making it easily excitable by a broad range of light at wavelengths below 558 nm, which covers a significant portion of the visible spectrum. Additionally, the conduction band of $Fe_2O_3$is ideally positioned at a lower energy level than that of TiO_2, giving it the ability to act as an electron acceptor capable of trapping photogenerated electrons from the conduction band of TiO_2following its excitation.Iron oxide typically exists in the +3 oxidation state, meaning Fe^{3+} ions are the active species in the coupled system. These ions possess an interesting property: they occupy a volume with a radius of 0.68 Å, nearly equal to that of Ti^{4+} (0.64 Å), allowing them to be incorporated into the TiO_2 matrix. Thus, iron in the form of Fe_2O_3presents a strong candidate for coupling with TiO_2 to reduce electron-hole recombination [29].Among various methods employed for the synthesis of composite semiconductor nanostructures, including dip coating[30], electrodeposition [31, 32], layer by layer assembly[33], atomic layer deposition [34] and impregnation method is widely used for the deposition of co-catalysts[35].This technique typically involves immersing TiO_2 samples into a suitably selected solution, followed by annealing under specific conditions to achieve thedesired crystalline structure of both oxides. In this approach, transition metal oxide can be deposited on walls and surface of the porous TiO_2 structure. A particularly promising strategy involves the incorporation of iron (III) oxide (Fe_2O_3), which is regarded as one of the most effective visible-light-driven semiconductors, owing to its

narrow band gap (~2.2 eV), low cost, non-toxicity, and high chemical stability [36].Upon light irradiation, photo-excited electrons from the valence band of Fe_2O_3can be effectively transferred to the conduction band of TiO_2, enhancing charge separation [37]. As previously reported, the morphological, structural,optical,and photoelectrochemical properties of Fe_2O_3-TiO_2 materials can significantly differ based on an impregnation process. For instance, Kuang et al. demonstrated the modification of anodic TiO_2 nanotubes by Fe_2O_3 by immersing them in an aqueous solutionof $FeCl_3$ and NaOH. After four successive immersion cycles, the samples were annealed at 550 °C for 4 h,resulting in the formation of crystalline anatase and hematite phases. The photoelectrochemical performance of synthesized materials under the white light illumination was enhanced about four times compared to pristine TiO_2 nanotubes [38].On the other hand, Jeon et al. [39] proposed a hybrid approach that combines two techniques for the synthesis of Fe_2O_3-TiO_2 structures: (i) impregnation of anodized TiO_2 in an iron (III) chloride solution, and (ii) electrochemical deposition.

I.10. Application of Fe_2O_3-TiO_2nanotubes (NTs)

Fe_2O_3-TiO_2 nanotubes (NTs) have gained significant attention in photocatalysis and renewable energy applications due to their enhanced charge separation efficiency, broad light absorption range, and reduced electron-hole recombination. Below are some applications:

- **Photocatalytic Water Splitting for Hydrogen Production**

The coupling of Fe_2O_3(α-Fe_2O_3hematite) with TiO_2 nanotubes improves visible-light absorption (Fe_2O_3 has a narrow band gap of ~2.2 eV).The staggered band alignment (Type-II heterojunction) facilitates electron transfer from the TiO_2 conduction band (CB) to Fe_2O_3, reducing charge recombination.This system enhances H_2 evolution under solar irradiation by efficiently utilizing photogenerated electrons for proton reduction ($H^+ \rightarrow H_2$)[35].

- **Environmental Remediation (Pollutant Degradation)**

The composite exhibits improved visible-light-driven photocatalytic activity for degrading organic pollutants (dyes, pharmaceuticals, pesticides).Fe^{3+}/Fe^{2+} redox cycles promote the generation of reactive oxygen species, enhancing degradation efficiency[40].

I.11. Conclusion

This literature reviewhas systematically examined the characteristics of titanium dioxide (TiO_2) and iron oxide (Fe_2O_3), including their optical behavior, electronic structure and electrical characteristics.The fundamental principles of photoelectrochemistry werepresented, establishing TiO_2 as the optimal material for photoelectrochemical water splitting applications. A primary focus was the photosensitization of TiO_2 through semiconductor coupling with Fe_2O_3, which enhances photocatalytic activity by extending light absorption into the visible spectrum, improving charge separation efficiency and reducing electron-hole recombination. The resulting Fe_2O_3-TiO_2 hetero-nanostructures provide the foundation for the experimental investigation detailed in the following chapter.

CHAPTER II

Samples Elaboration And Characterization

This chapter describes the experimental procedures used to prepare the studied materials. The firstsection details the synthesis of TiO_2 nanotubes via anodic oxidation (anodization) and the fabrication of Fe_2O_3-TiO_2/Ti heterostructures through impregnation. The second section presents the characterization techniques employed to analyze the physico-chemical and morphological properties of the synthesized materials.

II. Introduction

Titanium dioxide (TiO_2) has attracted significant interest due to its remarkable properties including chemical stability, photocatalytic activity, and non-toxicity. These characteristics make it a promising material for diverse applications, particularly in energy and environmental remediation. However, its performance can be further enhanced through structural and optical modifications.In this study, iron oxide (Fe_2O_3) was incorporated into TiO_2 nanotubes to improve theirphotoelectrochemicaland electronic properties. This experimental study aims to fabricate self-organized TiO_2 nanotubes via anodic oxidation (anodization), and subsequently decorate them with Fe_2O_3 nanoparticles using a controlled deposition process. To assess the material properties and performance, we employed multiple characterization techniques, including X-ray diffraction (XRD), UV-Vis spectroscopy, Raman spectroscopy, Scanning Electron Microscopy (SEM), and photoelectrochemical measurements. These analyses provide comprehensive insights intothe structural, optical, morphological, and photo-electrochemical properties of the synthesized Fe_2O_3-TiO_2 nanotubes system.

II.1. Synthesis of Fe_2O_3-TiO_2 Nanotubes

II.1.1. Materials and Chemicals

The following materials and reagents wereused in this study:

Table II.1: Chemical reagents and materials employed in the fabrication of Fe_2O_3-TiO_2NTs.

Material/ Chemical	Chemical Formula	Role
Titanium Sheet	Ti	Anodization Substrate
Distilled water	H_2O	Rinsing and electrolyte preparation
Silicon Carbide paper	-	Surface polishing(various grit sizes)
Platinum Electrode	Pt	Counter electrode
Oxalic Acid	$C_2H_2O_4$	Chemical polishing
Hydrofluoric Acid	HF	Anodization electrolyte
Iron (II) Chloride	$FeCl_2$	Iron precursor for Fe_2O_3 deposition
Sodium Hydroxide	NaOH	Precipitation agent for $Fe(OH)_3$ formation
Furnace	-	✓ TiO_2 nanotube crystallization ✓ Thermal conversion of $Fe(OH)_2$ to Fe_2O_3

II.1.2. Fabrication of Self-Organized Crystalline TiO_2 Nanotubes

This section describes the synthesis of self-organized crystalline TiO_2 nanotubes via anodic oxidation. The fabrication process consisted of four steps: (1) surface preparation, (2) electrolyte preparation, (3) anodization, and (4) post-treatment. Each step carefully optimized to obtain well-aligned TiO_2 nanotubes with controlled morphological properties.

II.1.2.1.Surface Preparation

The titanium surface was prepared through the following sequence:

- ✓ Mechanically polishing using silicon carbide abrasive papers (180-2000 grit) as shown in Figure II.1.
- ✓ Thorough rinsing with distilled water.
- ✓ Chemical etching in 5% oxalic acid ($C_2H_2O_4$) aqueous solution at 100°C for 2 hours.
- ✓ Final rinsing with distilled water followed by air drying.

This pretreatment ensures surface cleanliness and activation for subsequent uniform TiO_2 nanotube growth.

Figure II.1: Polishing using silicon carbide.

II.1.2.2.Electrolyte Preparation

The anodization electrolyte (aqueous solution) was prepared by mixing 5 ml of hydrofluoric acid (HF, 48%)with 45 ml of distilled water under constant stirring. This aqueous HF solution (10%) enables the controlled electrochemical dissolution required for TiO_2 nanotube formation.

II.1.2.3.Anodization Process

The electrochemical anodization (Figure II.2) performed under the following conditions:

- ❖ Use a titanium sheet as the anode (+)(working electrode).
- ❖ Use a platinum or a graphite plate as the cathode (-)(counter electrode).
- ❖ Apply a constant voltage of 20V for an hour at room temperature.

Figure II.2: Anodization Process.

II.1.2.4.Post-Treatment

After anodization, the as-prepared TiO_2 nanotubes are in an amorphous phase. To improve their structural stability and photocatalytic activity, the samples undergo thermal annealing to promote crystallization into the anatase phase. The annealing process is carriedout as follows:

- ➢ The anodized samplethoroughly rinsedwith distilled water to remove residual electrolyte and surface contaminants (Figure II.3a).
- ➢ Complete drying achieved via ambient air exposure.

➢ Thermal crystallization performed in a furnace at 450°C with a controlled heating rate of 5°C/min (Figure II.3b).

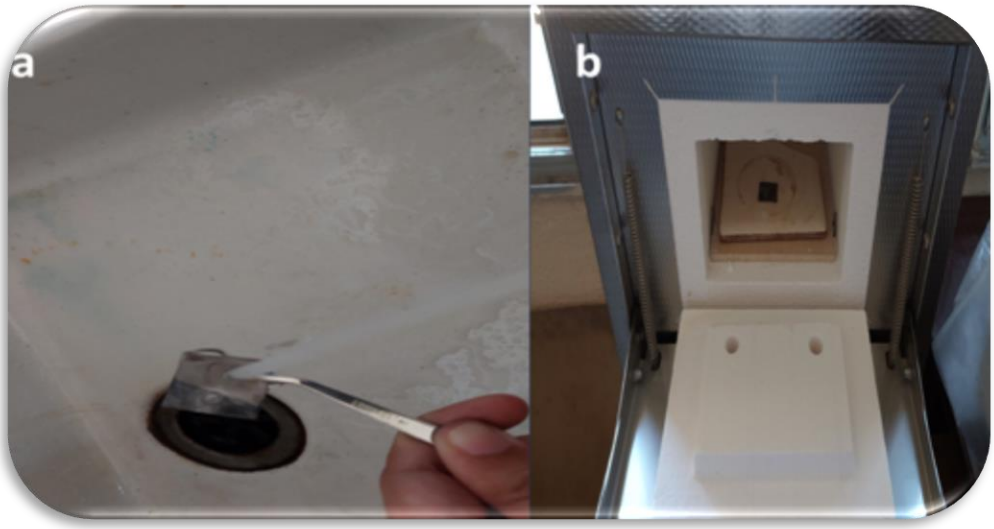

Figure II.3: Post-anodization processing of TiO_2NTs: (a) rinsing step; (b) thermal crystallization at 450°C.

The transformation process from amorphous to crystalline TiO_2 nanotubes involves the following chemical reactions during anodization and subsequent annealing:

Table II.2: Chemical reactions during TiO_2 nanotube formation via anodization and crystallization.

Step	Chemical Reaction
Titanium oxidation	$Ti_{(s)} \rightarrow Ti^{4+}_{(aq)} + 4e^-$ (II.1)
Water decomposition under applied potential	$2H_2O_{(l)} \rightarrow O^{2-}_{(aq)} + 4H^+_{(aq)} + 2e^-$ (II.2)
TiO_2 formation	$Ti^{4+}_{(aq)} + O^{2-}_{(aq)} \rightarrow TiO_{2(s)}$ (II.3)
TiO_2 dissolution by fluoride (composition of pores)	$TiO_{2(s)} + 6F^-_{(aq)} + 4H^+_{(aq)} \rightarrow [TiF_6^{2-}]_{(aq)} + 2H_2O_{(l)}$ (II.4)
Crystallization (annealing)	$TiO_{2(Amorphous)} \xrightarrow{450^\circ C} TiO_{2(Anatase)}$ (II.5)

S: solid, aq: aqueous, l:liquid

II.1.3.Preparation of Fe_2O_3-TiO_2Nanotubes

In this step, iron (III) oxide (Fe_2O_3) deposited onto the surface of previously synthesized TiO_2 nanotubes. The process involves the preparation of alkaline and iron salt solutions, followed by controlled immersion cycles to facilitate $Fe(OH)_3$ deposition and thermal treatment to convert $Fe(OH)_3$ to crystalline Fe_2O_3 and ensure strong interfacial adhesion

- **Fe_2O_3deposition protocol**

a. Solution Preparation

➢ Alkaline solution: 0.04 g NaOH dissolved in 10 *ml* distilled water (stirred until homogeneous).

➢ Iron precursor: 0.1622 g $FeCl_2$ dissolved in 10 *ml*distilled water (freshly prepared under nitrogen atmosphere to prevent oxidation to Fe^{+3}).

b. Cyclic deposition

- Immerse TiO_2 nanotubes in $FeCl_2$ solution (5 min), then rinse with distilled.
- Transfer to NaOH solution for 5 min, followed by a final rinse with distilled water (5 min).
- Repeat the cycle four times to ensure uniform deposition (Figure II.4).

Figure II.4: Cyclic deposition.

c. Thermal treatment

- Anneal at 550°C for 4 hours (static air, same furnace as TiO_2 crystallization).
- Heating rate: 5°C/min (consistent with previous protocol).

The principal chemical reactions involved in the Fe_2O_3 nanoparticle deposition onto TiO_2 nanotubes are systematically presented in Table II.3.

Table II.3: Chemical reaction mechanism for hematite (Fe_2O_3) deposition on anodized TiO_2 nanotubes.

Step	Chemical Reaction	Conditions
Precipitation	$FeCl_{2(aq)} + 2NaOH_{(aq)} \rightarrow Fe(OH)_{2(s)} + 2NaCl_{(aq)}$ (II.6)	Room temperature
Oxidation	$4Fe(OH)_{2(s)} + O_{2(g)} + 2H_2O_{(l)} \rightarrow 4Fe(OH)_{3(s)}$ (II.7)	Ambient conditions
Heat-Treatment	$2Fe(OH)_{3(s)} \rightarrow Fe_2O_{3(s)} + 3H_2O_{(g)}$ (II.8)	550°C, 4 hours annealing

II.2.Characterization techniques for Fe_2O_3- TiO_2Nanotubes

II.2.1.X-ray Diffraction (XRD)analysis

X-ray diffraction (XRD) serves as a fundamental characterization technique for crystalline phase identification. In this study, XRD was employed to investigate Fe_2O_3-TiO_2 NTs and assess their structural properties.

II.2.1.1. Principle

When a material is irradiated by an X-ray photon beam, it emits secondary radiation with a wavelength nearly identical to the incident beam (λ) - a phenomenon known as elastic scattering. When the scattering centers are structurally organized within the material, the scattered waves may undergo interference, giving rise to diffracted waves of significantly enhanced intensity, provided Bragg's Law is satisfied [41]:

$$n\lambda = 2d\sin\theta \qquad \text{(II.9)}$$

Where:

n : is the diffraction order (integer).

λ : is the wavelength of the incident X-ray beam,

d : is the interplanar spacing (distance between crystal planes),

θ : is the angle of incidence (Bragg angle).

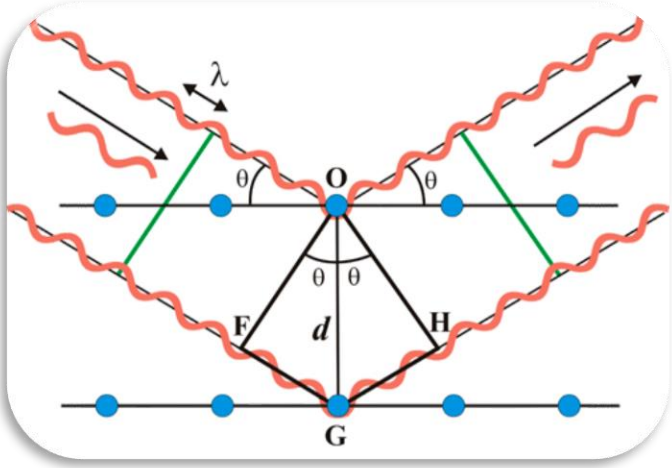

Figure II.5: Principle of X-ray diffraction by a Crystal and illustration of Bragg's Law [42].

II.2.1.2. Experimental Conditions

The sample was positioned at the center of a goniometer in Bragg-Brentano geometry.Diffraction patterns were recorded using a Panalytical Empyrean diffractometer equipped with:

- ✓ A multichannel Pixel detector.
- ✓ A copper X-ray source (λ(Kα) = 1.541874 Å).
- ✓ Operating parameters: 45 kV voltage and 40 mA current.
- ✓ The angular range is identical (20°-60°) with a step size of 0.07°.

The XRD instrument used in this study is illustrated in Figure II.6.

Figure II.6: Panalytical Empyrean Diffractometer.

II.2.2.Raman spectroscopy

Raman spectroscopy is widely used in chemistry because vibrational frequencies are directly linked to chemical bonds and molecular symmetry.These spectral features provide crucial insights intomolecular structure and material properties. This technique is complementary to infrared (IR) spectroscopy, offering additional capabilities for studying material vibrational modes. Raman spectroscopy is particularly valuable for analyzing nanomaterials such as TiO_2 NTs enhanced with Fe_2O_3 NPs, due to the following advantages [43]:

- ❖ Identification of crystalline phases (e.g., anatase or rutile in TiO_2 and hematite in Fe_2O_3).
- ❖ Monitoring structural changes induced by the incorporation of Fe_2O_3 into the TiO_2lattice.
- ❖ Verification of successful synthesis or chemical modification.

II.2.2.1.Principle

This spectroscopic technique operates a monochromatic light beam (typically from a laser source) onto the sample usinga lens system. The scattered light is then collected via a separate lens, directed through a monochromator, and detected by either:

- ✓ Single-channel detectors (photomultiplier tube or CPM)
- ✓ Multi-channel detectors (charge-coupled deviceor CCD).

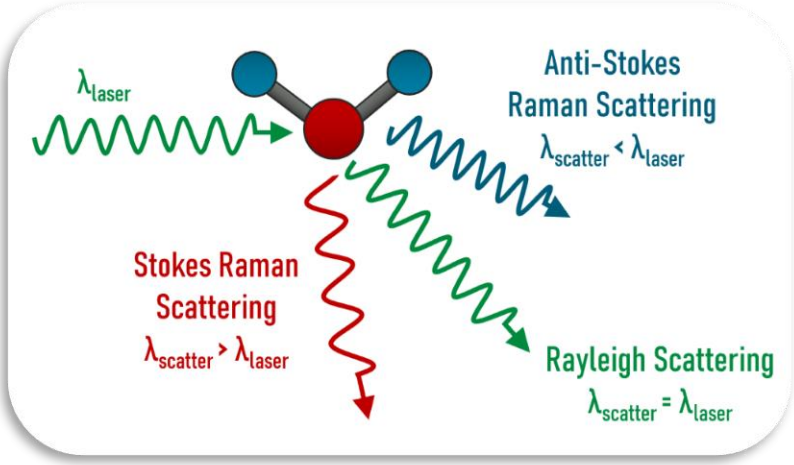

Figure II.7: Example of three different scattering mechanisms showing a given input wavelength compared with scattered wavelengths[44] .

II.2.2.2.Experimental conditions

The analysis was conducted using a Bruker SENTERA system (Figure I.8) with the following parameters:

- ✓ Excitation wavelength: 532 nm.
- ✓ Spectral range: 50-2000 cm^{-1}.
- ✓ Laser power: 20 mW.

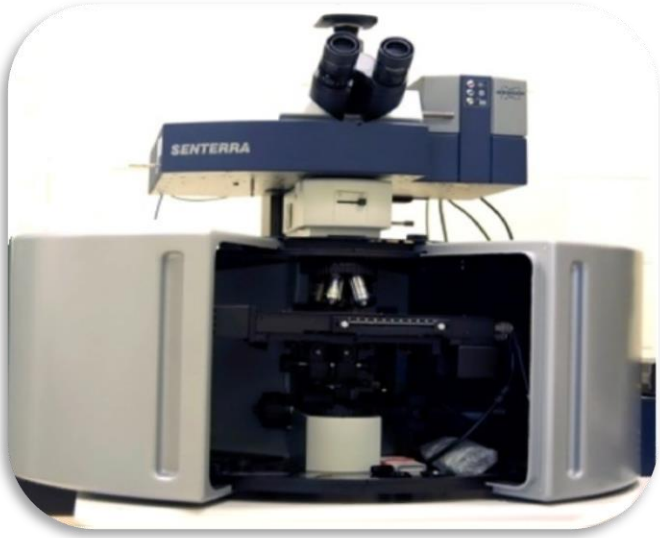

Figure II.8: Schematic of Raman spectroscopy instrumentation.

II.2.3.UV-Vis Diffuse Reflectance Spectroscopy (DRS)

UV-Visible spectrophotometry is a non-destructive optical characterization technique that provides information about the optical properties of the analyzed sample, such as light transmission, reflectance and absorption, estimation of the optical band gap and crystallite sizes. This technique can additionally yield data on sample thickness and even determine its optical constants [20, 45].

II.2.3.1.Principle

This technique analyzes the interaction between incident light (emitted or reflected) and the sample. The incident beam undergoes three possible interactions with the sample: Absorption, Transmission and Reflection. When a material absorbs ultraviolet or visible light (200-800 nm), the energy causes electronic transitions where electrons move from lower to higher energy states. These transitions occur in specific wavelength ranges (Ultraviolet region:200-400 nm and visible region:400-800 nm). For non-transparent samples, diffuse

reflectance spectroscopy measures the reflected light, providing crucial information about: the optical properties and absorption characteristics of the material [46].

II.2.3.2.Experimental conditions

In diffuse reflection mode, the instrument measures light scattered by the sample and that scattered by a reference, typically Teflon (the white standard). The device measures absorbance. Spectra wererecorded using aJasco ILN-725-V-676 diffuse reflectance spectrophotometerequipped with an integrating sphere coated with polytetrafluoroethylene (PTFE) for diffuse reflection measurements. The explored spectral range was between 200 and 800 nm.

Figure II.9: Jasco ILN-725-V-676 diffuse reflectance spectrophotometer.

II.2.3.3.Band Gap determination

UV-Visible spectroscopy analyzes the interaction between incident light and the sample, where the incident beam may be either absorbed or transmitted. When a substance absorbs light in the ultraviolet and visible ranges, the absorbed energy induces electronic transitions as electrons move from lower to higher energy states. As the samples were prepared as opaque pellets, measurements were conducted in reflectance mode. The reflectance data wassubsequentlyconverted to absorbance using the Kubelka-Munk function, enabling determination of the samples' optical band gap[47].

$$f(R_\infty) = \frac{(1-R_\infty)^2}{2R_\infty} = \frac{K}{S} = \frac{\varepsilon C}{S} \qquad \text{(II.10)}$$

Where:

R_∞: Absolute reflectance of an infinitely thick sample layer (diffuse reflectance).

$f(R_\infty)$: Kubelka-Munk function, relating reflectance to absorption and scattering properties.

K: Absorption coefficient of the sample.

S: Scattering coefficient of the sample.

ε: Molar absorptivity (extinction coefficient ($l \cdot mol^{-1} \cdot cm^{-1}$)), quantifies light absorption by a chemical species at specific wavelengths.

C: Concentration of the absorbing species ($mol \cdot l^{-1}$)

- **Kubelka-Munk Transformation for Band Gap Determination**

The Kubelka-Munk transformation converts reflectance spectrum into a conventional absorption-like spectrum, similar to that obtained from solution-phase measurements. In the case of samples adsorbed on an inert, non-absorbing substrate, the absorption coefficient Krepresents exclusively the adsorbate's absorption properties, and shows direct proportionality to the adsorbate concentration on the substrate.By extrapolating the linear portion of the curve $[F(R) \times h\upsilon]^n$ as a function of$h\upsilon$ (where $h\upsilon$is simply the photon energy E in eV) and the exponent n depends on the nature of the electronic transition (for allowed direct transitions,$(n = 2)$.So that the band gap value can be determined.

II.2.4.Scanning Electron Microscopy (SEM)

Scanning Electron Microscopy (SEM) is an essential analytical technique employed for high-resolution limitations inherent to optical microscopy, enabling detailed surface characterization with superior depth of field, higher magnification capabilitiesand resolution down to the nanometer scale Scanning.

II.2.4.1.Principle

In this technique, the surface of the analyzed material is bombarded under vacuum by a focused electron beam. The interactions between these electrons and the sample generate various signals, including secondary electrons and backscattered electrons emitted from the material surface. The detected intensity of these electrons depends on both the surface topography and the atomic weight of elements comprising the surface film. SEM images thus provide qualitative information about surface morphology (roughness, porosity) and composition[48].

II.2.4.2.Experimental conditions

In this study, imaging was performed using a field-emission gun scanning electron microscope (FEG-SEM, often abbreviated as MEB-FEG in Franco-English terminology). This advanced configuration enhances detection capability and resolution compared to conventional SEM systems. The instrument used was a JEOL JSM-7600 microscope operating at 2,5 kV.

Figure II.10:JEOL JSM-7600 microscope.

II.2.5.Photoelectrochemical (PEC) characterization

The PEC properties of the Fe_2O_3-TiO_2 composite will be systematically investigated under both illuminated and dark conditions. This comparative analysis will enable to measure the material's behavior in both conditions to determine the effect of illumination on its ability to generate electrical current and evaluate its performance in different environments.

II.2.5.1.Principle

The working principle of the Photoelectrochemical device is based on the use of a semiconductor material to convert solar energy into electrical energy through an electrochemical reaction. In this system, the working electrode made of Fe_2O_3-TiO_2 nanotubes absorbs light, exciting electrons and creating holes in the material. These electrons

then move to the electrochemical surface where they participate in oxidation or reduction reactions in the electrolyte solution. The resulting current from these reactions is measured using a potentiostat, allowing the study of the system's efficiency in generating solar energy. With this device, the effects of different lighting conditions on the electrochemical performance of the material can be studied, which helps improve the effectiveness of renewable energy electrochemical systems.

II.2.5.2.Photocurrent testing

This technique enables the determination of semiconductor type and its photoactivity. A depletion zone forms at the electrode surface when the semiconductor layer contacts the electrolyte. Due to the limited charge carriers available, the current remains very weak. Upon illumination of the electrode, electron-hole pairs are generated and separated within the space charge region, thereby producing a photocurrent. The amplitude of this photocurrent depends on[49]:

- ✓ Material properties.
- ✓ Deposition conditions.
- ✓ Applied potential.
- ✓ Electrolyte composition.

The photocurrent measurements were conducted using a Solartron Analytical SI 1287 Potentiostat/Galvanostat system, computer-controlled for experimental data acquisition. The setup employed a three-electrode electrochemical cell connected to the Potentiostat/Galvanostat (to control the applied potential and scan rate). The cell consisted of a 100 ml PYREX glass vessel configured with three electrodes. The potentiostat setup is illustrated in Figure II.11.The three-electrode system employed in this work consists of the following components:

- ➢ **Reference Electrode (RE):** used to measure the applied potential at the working electrode. The saturated Ag/AgCl was used as the reference, with a standard potential of +0.19 V vs. NHE (Normal Hydrogen Electrode) at 25°C.
- ➢ **Counter Electrode (CE):** a platinum (Pt) electrode arranged parallel to the working electrode to ensure uniform current distribution.
- ➢ **Working Electrode (WE):**TiO_2 NTs arrays and/or Fe_2O_3-modified TiO_2NTs composites were used for PEC measurements under Simulated solar illumination (AM 1.5G)

and dark conductions. 1M NaOH aqueous solution (Electrolyte) (80 *ml*) contained in a quartz electrochemical cell.

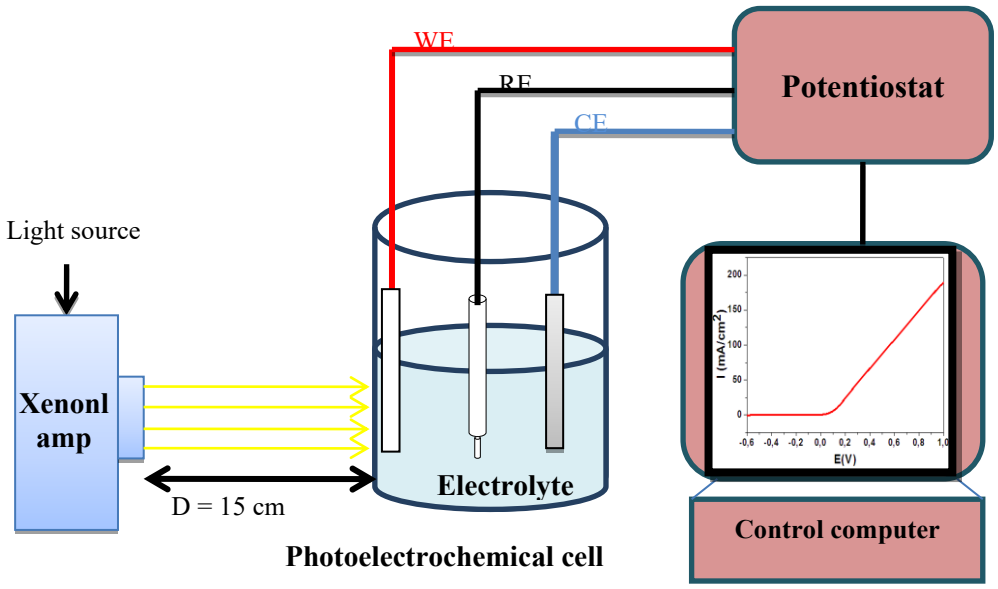

Figure II.11: Potentiostat experimental setup.

II.2.5.3.Electrochemical Impedance Spectroscopy

Electrochemical impedance spectroscopy (EIS) is a technique used to study electrochemical systems and analyze the kinetics of electrochemical processes. The physico-chemical properties of the system can be correlated with one or more components (resistances, capacitances, and inductances) of an equivalent electrical circuit to validate an electrochemical mechanism. From a more specific perspective, electrochemical impedance describes the response of an electrochemical system to an alternating current (AC) or voltage as a function of frequency. According to Ohm's law, impedance (Z) is expressed in ohms (Ω). Both resistance and impedance reflect the system's opposition to electron flow (current). In AC circuits, this opposition is termed impedance and can be decomposed into multiple factors.

In the case of an electrochemical cell, it can be inferred that: the charge transfer kinetics at the electrodes, the rate of chemical reactions at these electrodes, andthe diffusion of species from the solution to the electrodeconstitute minor resistive phenomena that collectively determine the system's total impedance [49].

Electrochemical impedance spectroscopy measurements were conducted in potentiostatic mode, and polarization curves were recorded to characterize the electrochemical

behavior of TiO_2 and Fe_2O_3-TiO_2NTs using a Solartron Analytical SI 1287 potentiostat controlled by Z_{View} software installed on a PC. The experimental setup was identical to that used for photocurrent measurements, employing the same cell and electrode configuration.

The EIS measurement parameters were as follows:

- ✓ **AC signal amplitude**: 10 mV.
- ✓ **Frequency range**: 100 kHz to 1 mHz.
- ✓ **Applied potential**: 0 V (open circuit potential, OCP).
- ✓ **Electrolyte:** 1 M NaOH.

II.3. Conclusion

This study demonstrates the critical role of complementary characterization techniques in nanomaterial analysis. The combination of physical characterization methods **(**X-ray diffraction, Raman spectroscopy, and UV-Visible reflectance spectroscopy) and electrochemical characterization techniques (photoelectrochemical measurements, electrochemical impedance spectroscopy) provides a comprehensive understanding of TiO_2 - Fe_2O_3 composite materials. This multi-scale characterization approach enables precise optimization of these hybrid systems for advanced applications in photocatalysis, solar energy conversion and environmental remediation.

CHAPTER III

Results and discussion

This chapter presents the physico-chemical characterizations of the synthesized materials in this work, focusing on the structural and optical properties of titanium dioxide nanotubes deposited on titanium metal plates via the anodization method. Additionally, it examines the effect of photosensitizing TiO_2 withiron (III) oxide (Fe_2O_3) nanoparticles, a modification that significantly enhances photo-responsiveness for target applications, particularly in photo-electrochemical water splitting for hydrogen production.

III.Introduction

This section analyzes the structural, optical, and electrical properties of the synthesized samples.The experimental data obtained through various techniques such as X-ray diffraction, Raman spectroscopy, and photoelectrochemical characterization, are systematically examined to elucidate the influence of titanium oxide (TiO_2) and iron oxide (Fe_2O_3) hybridization on the material's performance. Furthermore, the electrical behavior and optical properties of the samples are discussed, providing insights into their potential for advanced applications, particularly in photoelectrochemical systems.

III.1.X-ray Diffraction analysis

X-ray diffraction was employed to investigate the structural characteristics of TiO_2 nanotubes (NTs), in their as-prepared, annealed, and Fe_2O_3-modified states. The corresponding diffraction patterns are shown in the Figure III.1.

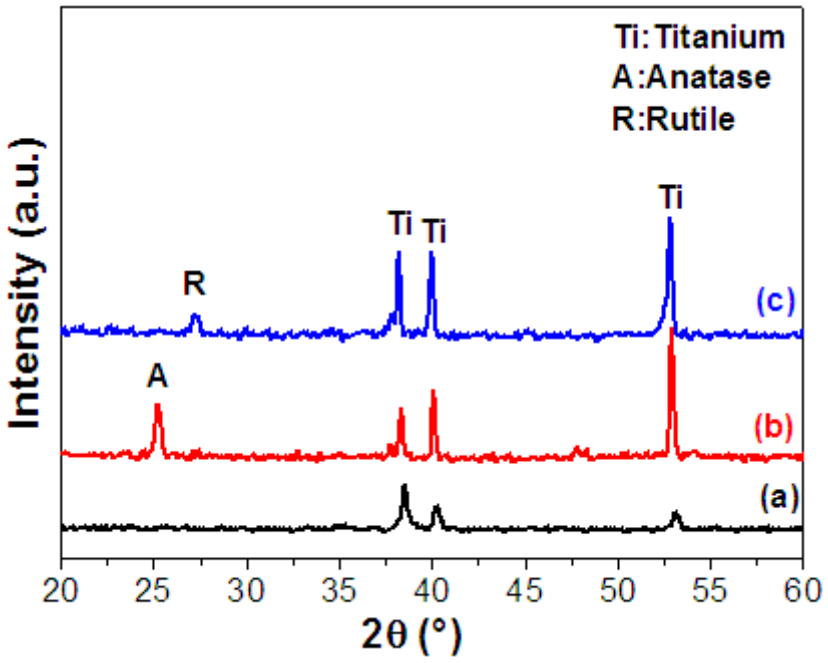

Figure III.1: XRD patterns of TiO_2 NTs arrays, (a) as-prepared amorphous TiO_2 NTs, (b) crystalline TiO_2 NTs after annealing at 450°C for 1 hour, and (c) Fe_2O_3-modified TiO_2 prepared via the impregnation method and annealed at 550°C.

For the as-prepared TiO_2NTs (Figure III.1a), diffraction peaks were observed at $2\theta = 38.54°$, 40.29° and 53.11°corresponding to the (002), (101), and (102) crystallographic planes of the titanium substrate (JCPDS No. 44-1294). The lack of distinct TiO_2–related

peaks in this pattern confirms the amorphous nature of the nanotubelayer before thermal treatment.

Following thermal treatment at 450°C (Figure III.1b), the previously amorphous TiO_2 NTs (which initially showed only Ti substrate reflections) crystallized into the anatase phase.This transformation was confirmed by the appearance of the characteristic (101) diffraction peak at $2\theta = 25.3°$ (JCPDS No. 21-1272), demonstrating successful conversion to a well-defined anatase structure. For Fe_2O_3-modified TiO_2 NTs prepared by impregnation and annealed at 550°C (Figure III.1c), the emergence of a peak at $2\theta = 27.3°$ corresponding to the (110) plane (JCPDS No. 21-1276) indicates partial phase transformation from anatase to rutile. This transition occurs because rutile-phase TiO_2, with its higher defect concentration, becomes thermodynamically favored at elevated temperatures or with impurity incorporation, thereby reducing the system's internal energy. Notably, no distinct Fe_2O_3 diffraction peaks were observed, suggesting that the iron oxide phase is present in low quantity, or highly dispersed, making it undetectable by conventional XRD analysis.

III.2.Raman spectroscopy analysis

The Raman spectra illustrated in the Figure III.2 provide a comparative analysis of pure TiO_2 nanotubes (TiO_2NTs) and Fe_2O_3-decorated TiO_2 NTs. The non-modified sample (Figure III.2a) exhibits characteristic vibrational modes of anatase TiO_2, with prominent peaks at 147.4, 197, 398.5, 519.7, and 636.5 cm^{-1}, corresponding to E_{g1}, E_{g2}, $B1_{g1}$, $B1_{g2}$ and E_{g3} symmetry modes [50, 51]. Upon decoration by Fe_2O_3(Figure III.2b), additional peaks appear at 242.6, 450.6 and 615 cm^{-1}, attributed to the rutile phase of TiO_2[52], as well as at 221, 294.9, and 1315 cm^{-1}, which correspond to α-Fe_2O_3(hematite) [51, 53]. These spectral features confirm the successful formation of a mixed-phase system involving anatase, rutile, and hematite.The comparison shows that the TiO_2 nanotubes are composed of pure anatase, while TiO_2 NTs decorated with Fe_2O_3 NPs are a mixture of anatase and rutile. This evolution is most likely due to the processing conditions of the Fe_2O_3-TiO_2/Ti, as the stabilization of hematite NPs requires an additional annealing at 550°C [54].As shown in Figure III.2, the peaks were sharp and well-developed, implying that the sample was well-crystallized in accordance with the XRD results. The presence of anatase, rutile TiO_2 and α-Fe_2O_3 peaks in samples of Fe_2O_3-TiO_2 in Figure III.2 confirms the heterostructures successful well formation. It is obvious fromthat the intensity of the peaks related to anatase TiO_2 was decreased in addition to observable broadening that is related to decrease in size of the

composite. This decrease in size can lead to an increase in the photocatalyst activity. Such structural transformation is consistent with previous studies. For example, Peng Luan et al. [55] reported that Fe_2O_3 loading induces the appearance of rutile TiO_2 modes even in systems originally dominated by the anatase phase, attributed to thermally induced phase transitions and Fe^{3+} ion diffusion into the TiO_2 nanorod. Multi-phase systems are known to exhibit enhanced charge separation, suppressed electron-hole recombination, and broader light absorption.

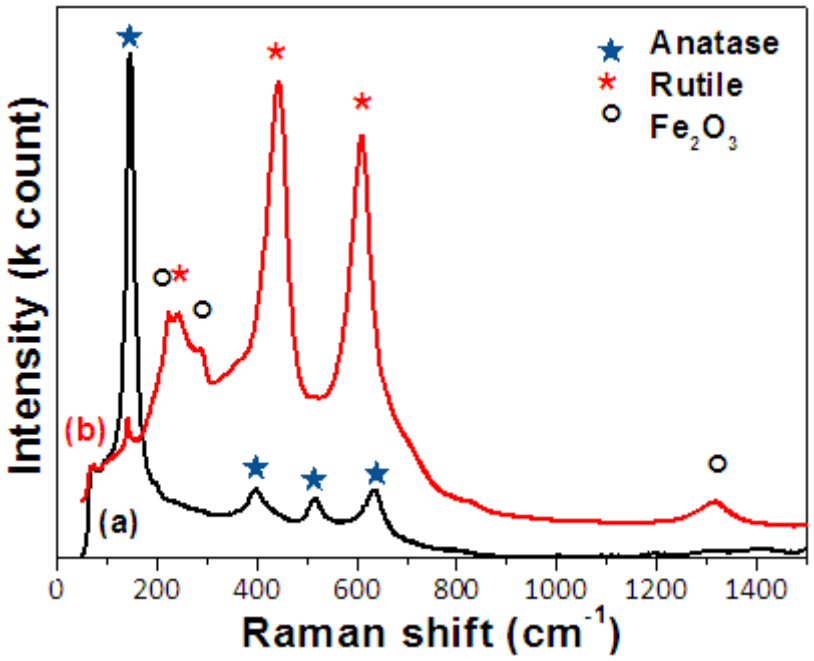

Figure III.2: Raman spectra of (a) bare TiO_2 NTs arrays and (b) Fe_2O_3- modifiedTiO_2 NTs prepared via CBD method.

III.3.SEM analysis

The SEM image of the TiO_2 NTs formed on the Ti substrate by anodization method is shown in Figure III.3a, The image demonstrates the formation of a highly dense and well-ordered array of TiO_2 NTs, exhibiting uniform tubular morphology with vertical alignment. These nanostructures were synthesized throughanodization of titanium in a fluoride-based electrolyte, a process that enables the self-organization of these hollow, architecturally regular nanotube arrays. Following chemical bath deposition (CBD) using an iron precursor and subsequent thermal treatment, Figure III.3b reveals the surface morphology of Fe_2O_3 nanoparticles deposited on the TiO_2 nanotube template. The SEM image distinctly shows the preserved architecture of vertically aligned TiO_2 nanotubes, maintaining their characteristic

highly ordered array structure. Notably, the nanotube surfaces are decorated with bright, granular features corresponding to Fe_2O_3nanoparticles. These nanoparticles demonstrate relatively uniform dispersion across the nanotube walls, confirming successful formation of a Fe_2O_3-TiO_2 heterostructure. Complementary EDS analysis (Figure III.3c) verifies the presence of iron in the modified samples, providing further evidence of Fe_2O_3 incorporation within the TiO_2 nanotube matrix.

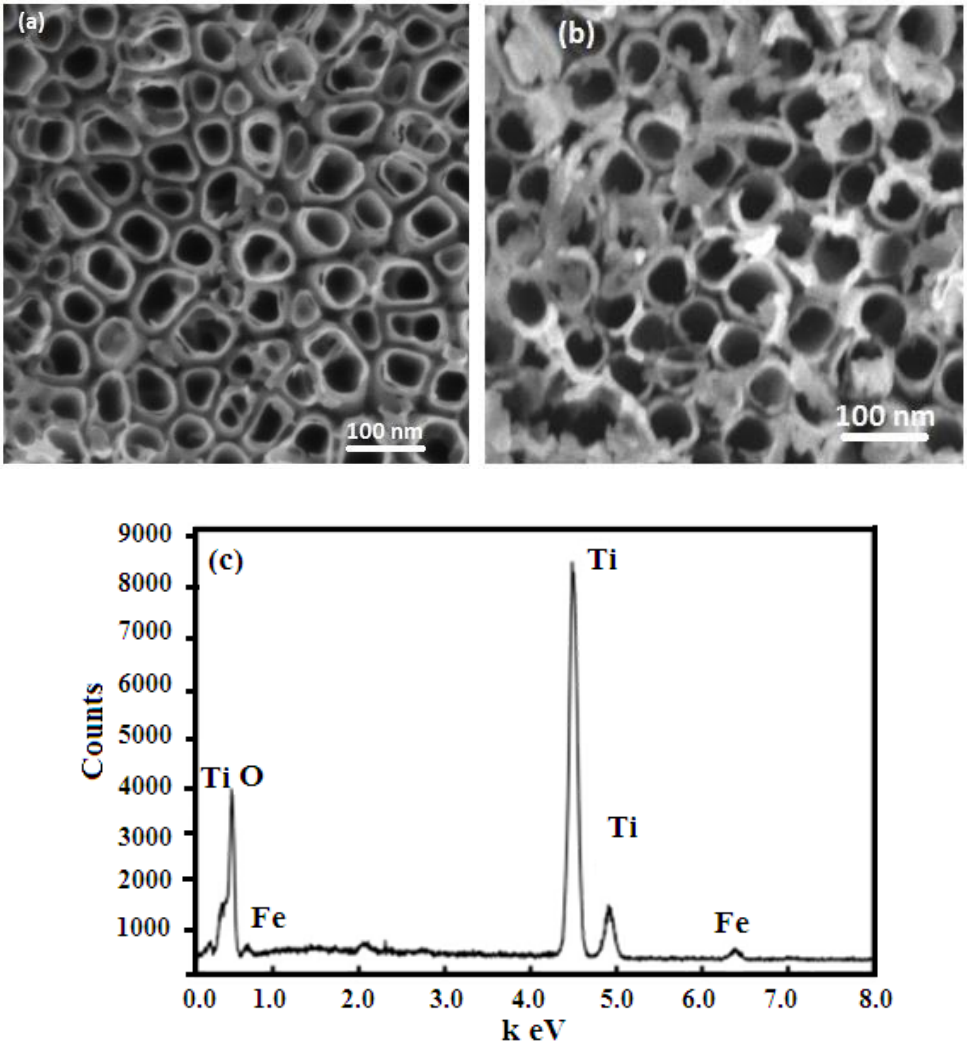

Figure III.3: SEM images showing: (a) top-view of as-prepared TiO_2 nanotube arrays, (b) Fe_2O_3-modified TiO_2 NTs prepared via impregnation, and (c) corresponding energy-dispersive X-ray spectroscopy (EDS) analysis of the Fe_2O_3-TiO_2 NTs.

III.4.UV-Vis DRS analysis

The Figure III.4 shows the diffuse reflectance spectra of pristine TiO_2 nanotubes (Figure III.4a) and Fe_2O_3-decorated TiO_2 nanotubes (Figure III.4b) recorded across the 200–800 nm wavelength range.

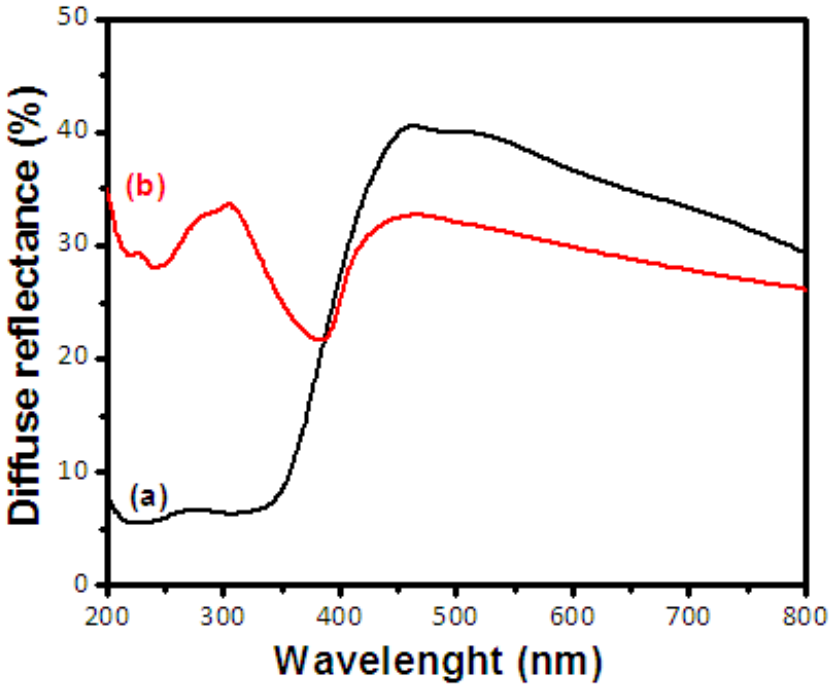

Figure III.4: UV-Vis diffuse reflectance spectra of (a) TiO_2 nanotubes arrays and (b) Fe_2O_3-modified TiO_2 NTs prepared via CBD method with subsequent annealing at 550°C.

The Figure III.4a indicates that the pristine TiO_2 NTs exhibit a characteristic absorption edge at 380-400 nm, corresponding to the intrinsic bandgap absorption of anatase-phase TiO_2 ($E_g \approx 3.2$ eV). This sharp reflectance increase is typical for wide bandgap semiconductors that primarily absorb in the UV region. In contrast, the Fe_2O_3-TiO_2NTs sample (Figure III.4b) display a pronounced red-shift of the absorption edge toward visible wavelengths, reduced overall reflectance in the UV range, and broader absorption features compared to pure TiO_2. The shift of the absorption edge toward longer wavelengths (red-shift) indicates an enhanced absorption in the visible light region, which is attributed to the incorporation of Fe_2O_3. Hematite (α- Fe_2O_3) is a narrow-band-gap semiconductorand its introduction results in a reduction in the overall band gap of the composite material.This enhanced visible light absorption suggests improved light-harvesting capability and may lead to superior photocatalytic or photoelectrochemical performance for the Fe_2O_3-TiO_2NTs compared to the pure TiO_2NTs.This behavior results from the integration of hematite (Fe_2O_3), a narrow band gap semiconductor, with titanium dioxide nanotubes. This hybrid structure contributes to a red shift in the absorption edge, expanding the absorption range toward longer wavelengths, and improves light-harvesting efficiency through better charge separation and reduced electron-hole recombination.

➢ **Optical Band Gap determination via Kubelka-Munkanalysis**

From the linear portion of the plot, a straight line was extrapolated to intersect the photon energy axis. This intersection point corresponds to the optical band gap value of the studied samples.

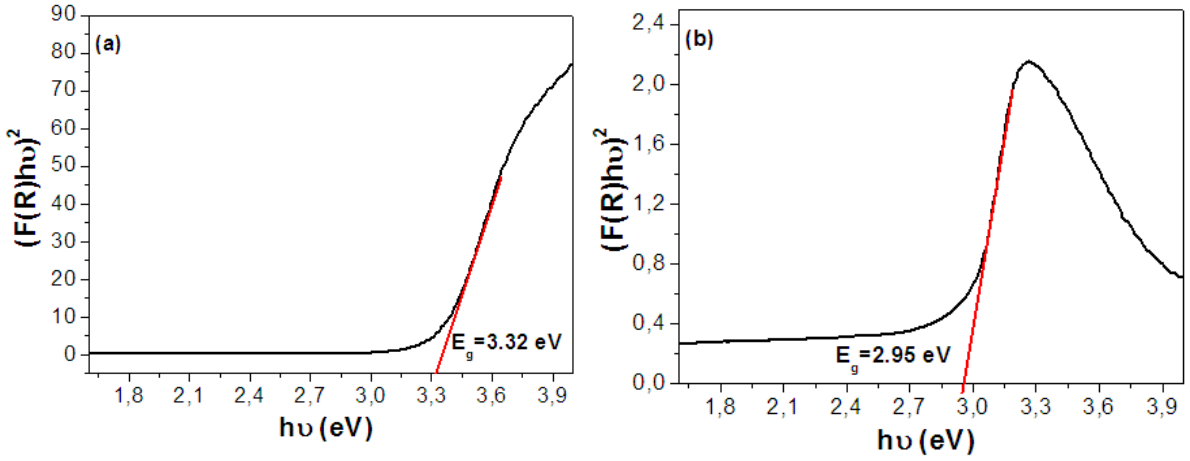

Figure III.5: (a) Determination of the band gap of TiO_2, and (b) of the Fe_2O_3-TiO_2 NTs.

The Kubelka-Munk plots revealed that the optical band gap of the TiO_2 NTs sample was approximately 3.32 eV, which is consistent with the typical wide band gap of pristine TiO_2NTs. In contrast, the hybrid Fe_2O_3-TiO_2NTs sample exhibited a noticeable reduction in band gap, estimated at 2.95 eV. This decrease can be attributed to the incorporation of Fe_2O_3, which improves visible light absorption and consequently enhances the photoelectrochemical and/or photocatalytic performance of the modified sample.

III.5.Photoelectrochemical properties of Fe_2O_3-TiO_2 NTs

The PEC test is carried out on the prepared samples but the best results were obtained with TiO_2 NTs decorated with Fe_2O_3 using the impregnation method which is consistent with what is observed with UV-vis diffuse reflectance given in Figure III.4, where the strongest light absorption occurs for the sample prepared by the impregnation process. Thus, only the PEC results related to the decoration by impregnation are presented here.

III.5.1.Comparison of PEC properties between TiO_2 and Fe_2O_3-TiO_2 NTs

Figure III.6 presents a comparative analysis of the photoelectrochemical performance of TiO_2 NTs and Fe_2O_3-decorated TiO_2 NTs electrodes in 1M NaOH electrolyte, as measured through linear sweep voltammetry. The current density (I, mA/cm²)is plottedas a function of

applied potential (E vs. Ag/AgCl, V), was comparing three experimentalconditions: TiO_2 NTs under dark conditions, TiO_2 NTs, and Fe_2O_3-TiO_2 NTs bothunder illumination.

Under dark conditions, TiO_2 NTs exhibit minimal current density across the appliedpotential range (-1.0 to 0.9 V vs. Ag/AgCl), confirming the material's inherent semiconductor properties. Upon illumination, TiO_2 NTs demonstrate a significant increase in current density, particularly at negative potentials (red curve, Figure III.6b), characteristic of n-type semiconductor behavior and indicating photoinduced charge carrier generation. In addition, the TiO_2 NTs show a pronounced cathodic photocurrent onset at approximately -0.68 V, reaching a saturation current density of 0.43 mA/cm² at 0.9 V, which aligns with the material's known bandgap (3.32 eV) and charge carrier dynamics [56].

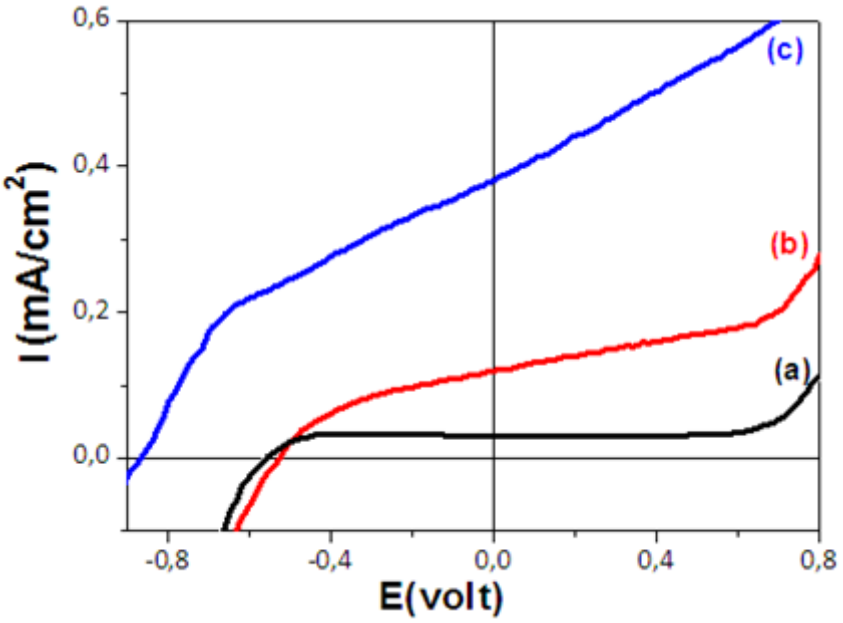

Figure III.6: Current–potential characteristics in 1 M NaOH solution for bare TiO_2 NTs arrays in the dark (a) and under simulated solar light (b), and for Fe_2O_3-TiO_2 NTs under simulated solar light (c).

❖ **Enhanced PEC Performance of Fe_2O_3-TiO_2 NTs**

The Fe_2O_3-TiO_2NTs electrode demonstrates significantly photoelectrochemical activity, exhibiting higher current densities across the entire potential window compared to pristine TiO_2 NTs under illumination. Notably, the photocurrent at 0.0 V shows a threefold increase following Fe_2O_3 decoration relative to bare TiO_2 NTs. The photocurrent enhancement can be attributed to the improvement of charge separation as a consequence of the decoration with Fe_2O_3. This improvement can be attributed to several factors: extended light absorption into

the visible spectrum due to the narrower band gap of Fe_2O_3, and improved charge separation efficiency at the Fe_2O_3-TiO_2 heterojunction interface. The observed performance improvement can be attributed to the formation of a type-II heterojunction, which facilitates electron-hole separation while reducing recombination losses.

The stability of the photocurrent plateau at anodic potentials (> 0.4 V) suggests effective hole transfer to the electrolyte interface, a critical factor for practical photoelectrochemical applications. This enhanced performance positions Fe_2O_3-TiO_2NTs heterostructures as promising photoanodes for solar water splitting applications, particularly when paired with co-catalysts for the oxygen evolution reaction [55, 57].

The photoelectrochemical performance of Fe_2O_3-TiO_2NTs heterostructure (in this study) shows significant advancements compared to previous reports in the literature. While the Fe_2O_3-TiO_2NTs in our system demonstrate a photocurrent density of 0.51 mA/cm² at 0.4V, this value exceeds the 0.3 mA/cm² range reported for similar Fe_2O_3-TiO_2 NRs arrays in alkaline media by Luan et al. [55], likely due to optimized nanotubes morphology and improved crystallinity in this fabrication process.This is evidenced by the results of chronoamperometry measurements (On/Off) were performed to evaluate the efficiency of charge separation and chemical stability.

III.5.2.Photocurrent performance of TiO_2 and Fe_2O_3–TiO_2 NTs (On/Off Cycles)

Figure III.7shows the photocurrent density as a function of time for the as-prepared TiO_2 and Fe_2O_3-TiO_2 electrodes under periodic light irradiation at a bias potential of 0.0 V (vs. Ag/AgCl). The light illumination was controlled with a 20/20 second light/dark cycle. Both materials exhibit a rapid photocurrent response when exposed to light, followed by stabilization. It is clearly observed that after several on–off irradiationcycles. In addition,both samples exhibit a good reproducibility and stability. Certainly, the photocurrent rapidly increases when the light is turned “ON” and immediately returns to zero when the light is turned “OFF”.The Fe_2O_3-TiO_2 NTs demonstrate a significantly higher photocurrent density (reaching 0.04A/cm^2) compared to the pristineTiO_2 NTs (reaching 0.01A/cm^2) throughout the entire time range (0-500s), indicating enhanced photoactivity due to iron oxide modification.This enhancement in photocurrent density is attributed to the reduced recombination rate of photogenerated charge carriers and more efficient generation of electron-hole pair under lower energy visible light as well [50, 58], revealing the efficient

photo-induced charge transfer between Fe_2O_3 and TiO_2 [59]. Also, improved performance suggests that the Fe_2O_3-TiO_2 heterostructures facilitates more efficient charge separation and electron transport, making it particularly suitable for photo-electrochemical applications such as water splitting or solar energy conversion. The stable photocurrent response over time also highlights the material's durability under continuous illumination. These results demonstrate that incorporating Fe_2O_3 into TiO_2NTs effectively boosts their photoelectrochemical performance.

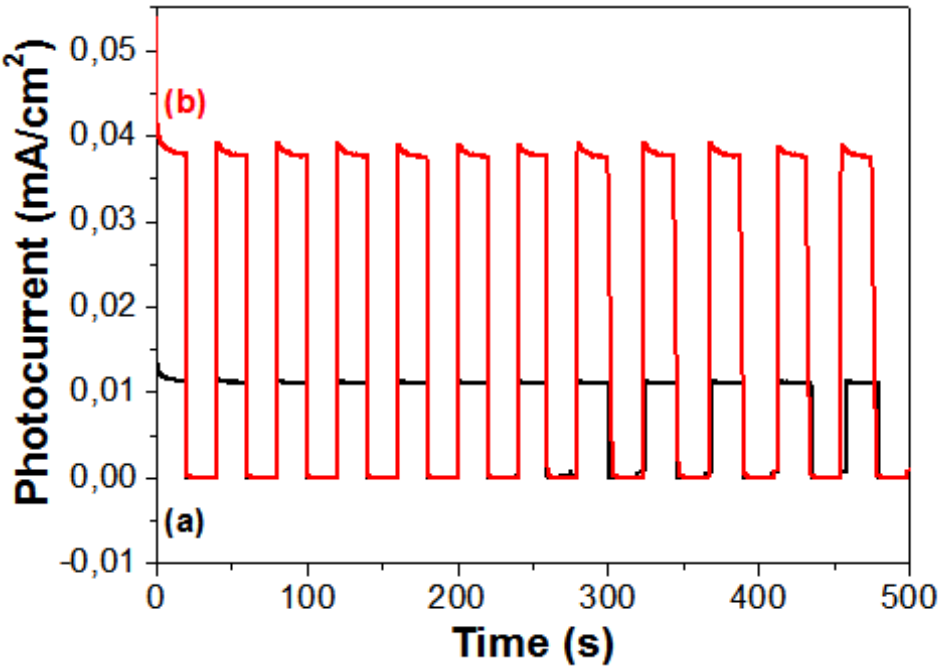

Figure III.7: Transient photocurrent response under choppedillumination at 0V vs. Ag/AgCl for pristine TiO_2 NTs (a) and Fe_2O_3-TiO_2 NTs samples (b) in 1 M NaOH electrolyte.

III.6.Electrochemical impedance spectroscopy(EIS)analysis of TiO_2 and Fe_2O_3-TiO_2NTs

EIS measurements were performed on both TiO_2 and Fe_2O_3-TiO_2 electrodes in 1 M NaOH electrolyte. An alternating current (AC) voltage of 10 mV was applied over a frequency range from 1 Hz to 100 kHz. The Nyquist plot comparison between pristine TiO_2 NTs and Fe_2O_3-modified TiO_2NTs reveals significant differences in charge transfer behavior. The pure TiO_2 sample exhibits a large semicircular arc in the high-frequency region, indicative of a high charge transfer resistance (R_{ct}) at the electrode-electrolyte interface. This is characteristic of limited electron mobility and inefficient interfacial charge transfer in unmodified TiO_2. In contrast, the Fe_2O_3-TiO_2NTselectrode demonstrates a significantly reduced semicircle diameter, reflecting enhanced charge transfer efficiency due to the synergistic effects of the heterojunction formation. This improvement can be attributed to

three factors: (1) the narrower band gap of Fe_2O_3 extending light absorption into the visible spectrum, (2) improved charge separation at the Fe_2O_3-TiO_2 interface and (3) increased surface active sites for electrochemical reactions.

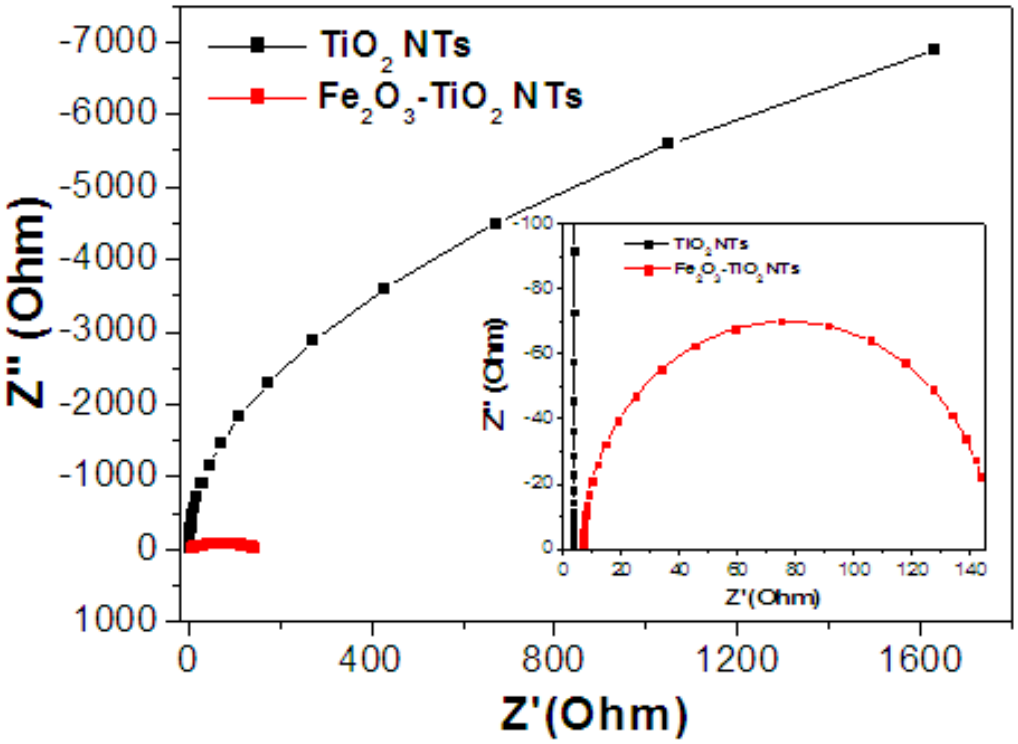

Figure III.8: Nyquist plots of TiO_2 and Fe_2O_3-TiO_2NTs electrodes recorded in 1M NaOH.

For the Fe_2O_3-TiO_2electrode, a well-defined semicircle wasobserved, allowing the determination of the series resistance (Rs), which was found to be 6.65 Ω. The end of the semicircle reached 142.82 Ω, resulting in a calculated charge transfer resistance (R_{ct}) of approximately 136.17 Ω. These values indicate relatively good electrochemical performance, with acceptable charge transfer at the electrode/electrolyte interface, attributed to the improved conductivity due to the incorporation of Fe_2O_3 into TiO_2.

III.7.Conclusion

This chapter systematically investigatesthe physico-chemical characterizations of TiO_2 nanotube arrays (NTs) and their Fe_2O_3-modified counterparts through comprehensive characterization.The scanning electron microscopy study shows that theanodized TiO_2 maintains well-defined nanotubular architecture and Fe_2O_3 nanoparticle deposition preserves the nanotube framework while increasing surface density. Characterization by diffuse

reflection shows that the addition of NPs can improve the absorption of TiO_2 NTs in the visible light range. Raman spectroscopy characterization was performed on TiO_2 and Fe_2O_3-TiO_2NTs. The Raman spectra confirm the anatase nature of the TiO_2NTs and establish the hematite nature of the deposited ferric oxide. The photoelectrochemical results show that the photocurrent is improved following the deposition of Fe_2O_3 NPs in the Fe_2O_3-TiO_2 hetero-nanostructure.The synergistic combination of structural characterization and functional measurements validates Fe_2O_3-TiO_2 NTs as an efficient visible-light-responsive photocatalyst system.

General conclusion

General Conclusion

This research successfully achieved its objectives to fabricate photosensitive α-Fe_2O_3-TiO_2 NTs heterostructures, characterize their structural and functional properties, and evaluate their performance in photoelectrochemical applications.

Two distinct nanostructured materials (TiO_2NTs and Fe_2O_3-modified TiO_2NTs) were synthesized and characterized in this study. The TiO_2 nanotubes were fabricated using the anodization technique of Ti foil, a controlled electrochemical method known for producing highly ordered and vertically aligned tubular nanostructures. The Fe_2O_3-TiO_2heterostructures were subsequently synthesized through chemical bath deposition (CBD) process employed the iron (III) chloride precursor solution, followed by thermal treatment at 550°C for 2 hoursto deposit Fe_2O_3nanoparticles.

This study aimed to develop nanostructured materials with precisely controlled properties, particularly concerning crystal size, morphology (highly ordered and vertically aligned tubular), and especially the electronic and optical properties, which play a very important role in the water photo-electrolysis applications carried out. Two methodologies were employed for the preparation of nanostructures based on TiO_2NTs and Fe_2O_3 NPs, exhibiting varied and controlled properties:

- Firstly, the preparation of titanium dioxide with nanotubes morphologies using the anodization method, which consists of introducing the reactants into a three-electrode cell, with the entire setup placed under a potential of 20V for 1 hour. This process facilitates the formation of uniform and vertically aligned nanotube arrays with high surface area and structural integrity.

- Secondly, Fe_2O_3nanoparticles were deposited onto the pre-formed TiO_2NTs by immersing the nanotube films into an aqueous solution containing the iron precursor, followed by thermal treatment. This straightforward method enables the formation of Fe_2O_3-TiO_2/Ti heterostructure.
- Finally, the photoelectrochemical performance of the synthesized nanomaterials was evaluated using a solar simulator and a potentiostatic system. These tests were designed to assess the materials' efficiency in harvesting solar energy and generating photocurrent, thereby determining their suitability for hydrogen production via photoelectrolysis of water.

References

References:

[1]A. BRAYEK, "Étude des Propriétés Photo-Électrochimiques des Structures Cœur-Coquille ZnO/ZnS Électro-déposées sur Verre/ITO", PhD Thesis, University of Manar, Tunisia, 2016.

[2]M. A. Kumar et al., "Recent trends in photoelectrochemical water splitting: the role of cocatalysts", Journal: NPG Asia Materials, 14, 88, 2022.

[3]M. El Ouardi et al., "Review of photoelectrochemical water splitting: From quantitative approaches to effect of sacrificial agents, oxygen vacancies, thermal and magnetic field on (photo) electrolysis", Journal: International Journal of Hydrogen Energy, 69, 760–776, 2024.

[4] M. Yu et al., "Preparation and characterization of mesoporous TiO_2-Fe_2O_3 composite films with enhanced visible light photocatalytic activity", Journal: Journal of Porous Materials, 20, 285–292, 2013.

[5] N. Tabaja, "Nanoparticules d'oxyde de fer et de ferrites obtenues par nano-réplication: réactivité chimique et application en dépollution des eaux", PhD Thesis, Pierre and Marie Curie University – Paris 6, 2015.

[6] C.E. Ekuma and D. Bagayoko, "Ab-initio electronic and structural properties of rutile titanium dioxide", Journal: Japanese Journal of Applied Physics, 50, 05JC05, 2011.

[7] H. Zennir, "Étude des propriétés photo-électrochimiques de nano-fibres de TiO_2 photo-sensibilisées par des quantum dots de CdSe", Master Thesis, University of 20th August 1955, Skikda, 2017.

[8] N. Cheridi, "Étude des propriétés photo-électrochimiques de ZnSe–TiO_2 hétéro-nanostructures", Master Thesis, University of 20th August 1955, Skikda, 2018.

[9] B. Chavillon, "Synthèse et caractérisation d'oxydes transparents conducteurs de type p pour application en cellules solaires à colorant", PhD Thesis, University of Nantes, France, 2011.

[10]H. Ishaqet al., "A review on hydrogen production and utilization: Challenges and opportunities", International Journal of Hydrogen Energy", 47, 26238-26264, 2022.

[11] H. H. Shanaah et al., "Photocatalytic Degradation and Adsorptive Removal of Emerging Organic Pesticides Using Metal Oxide and Their Composites: Recent Trends and Future Perspectives", Journal: Sustainability, 15, 7336, 2023.

[12] O. U. Akakuru, Z. M. Iqbal, and A. Wu, "TiO_2 Nanoparticles, Applications in Nanobiotechnology and Nanomedicine", Wiley, 2020.

[13] O. Benkhetta, "Effet de la concentration de la solution sur les propriétés des couches minces de dioxyde de titane déposées par spray pyrolyse ultrasonique", Master Thesis, University of Mohamed Khider, Biskra, Algeria, 2019.

[14] H. Peng et al., "First-principles study of the electronic structures and magnetic properties of 3d transition metal doped anatase TiO_2", Journal: Journal of Physics: Condensed Matter, 20, 105203, 2008.

[15] D. Lalaoui, "Study of the Photoelectrochemical Properties of CdS-TiO_2/Ti Nano-Hybrids", Master Thesis, University of 20thAugust, 1955, Skikda, Algeria, 2020.

[16] X. Chen et al., "Titanium Dioxide Nanomaterials: Synthesis, Properties, Modifications, and Applications", Journal: Chemical Reviews, 107, 2891–2959, 2007.

[17] M.A. Gatou et al., "Photocatalytic TiO_2-Based Nanostructures as a Promising Material for Diverse Environmental Applications: A Review", Journal: Reactions, 5, Pages 135–194, 2024.

[18] G. Pfaff et al., "Angle Dependent Optical Effects Deriving from Submicron Structures of Films and Pigments", *Chemical Reviews*, 99, 1963–1982, 1999.

[19] D. Regonini, "AnodisedTiO_2 Nanotubes: Synthesis, Growth Mechanism and Thermal Stability", PhD Thesis, University of Bath, UK, 2008.

[20]A. Osman et al., "Hydrogen production, storage, utilization and environmental impacts: a review", Environmental Chemistry Letters, 20, 153–188, 2021.

[21] J. B. Ward, "The colouring and working of the refractory metals Titanium, Niobium and Tantalum for jewellery and allied applications", Report N.35/1, the Worshipful Company of Goldsmiths, 1982.

[22] Y. T. Sul et al., "Bone Incorporation in Retrieved Clinical Oral Implants: A Study of Histomorphometry and Removal Torque", Journal: Journal of Materials Science: Materials in Medicine, 12, 455–462, 2001.

[23] G. Hodes, "Semiconductor and Ceramic Nanoparticle Films Deposited by Chemical Bath Deposition", Journal: Physical Chemistry Chemical Physics, 9, 2181–2196, 2007.

[24] T.Schneller, R. Waser, M. K. Rühle, and U. Poppe, "Chemical Solution Deposition of Functional Oxide Thin Films", Springer Vienna, 2013.

[25] P. K. Nair et al., "Semiconductor Thin Films by Chemical Bath Deposition for Solar Energy Related Applications", Journal: Solar Energy Materials and Solar Cells, 51, 95–111, 1998.

[26] J. A. Switzer et al., "Electrodeposition and Chemical Bath Deposition of Functional Nanomaterials", Journal: MRS Bulletin, 35, 743–750, 2010.

[27] L. Pauling et al., "The Crystal Structures of Hematite and Corundum", Journal: Journal of the American Chemical Society, 47, 781–790, 1925.

[28] P. Hiralal et al., "Nanostructured Hematite Photoelectrochemical Electrodes Prepared by the Low Temperature Thermal Oxidation of Iron", Journal: Solar Energy Materials and Solar Cells, 95, 316–324, 2011.

[29] M. Ismail, "Préparation et caractérisation de nouveaux matériaux pour la décontamination de l'eau par photocatalyse sous lumière visible", PhD Thesis, National Polytechnic Institute of Lorraine (INPL), France, 2011.

[30] A. I. Kontos et al., "Self-organized Anodic TiO_2 Nanotube Arrays Functionalized by Iron Oxide Nanoparticles", Journal: Chemistry of Materials, 21, 954–962, 2009.

[31] Y. Liu et al., "Anodized TiO_2 Nanotubes Coated with Pt Nanoparticles for Enhanced Photoelectrocatalytic Activity", Journal of Materials Research, 32, 757–765, 2017.

[32] H. Park et al., "Electrodeposition of Maghemite (γ-Fe_2O_3) Nanoparticles", Journal: Chemical Engineering Journal, 139, 208–212, 2008.

[33] Y. G. Guo et al., "TiO_2-Based Composite Nanotube Arrays Prepared via Layer-by-Layer Assembly", Journal: Advanced Functional Materials, 15, 1859–1865, 2005.

[34] J. P. Niemelä et al., "Titanium Dioxide Thin Films by Atomic Layer Deposition: A Review", Journal: Semiconductor Science and Technology, 32, 013002, 2017.

[35] J. F. Guayaquil-Sosa et al., "Hydrogen Production via Water Dissociation Using Pt–TiO_2 Photocatalysts: An Oxidation–Reduction Network", Journal: Catalysts, 7, 278, 2017.

[36] J. Q. Li et al., "Preparation, Characterization and Visible-Light-Driven Photocatalytic Activity of Fe-Incorporated TiO_2 Microspheres Photocatalysts", Journal: Applied Surface Science, 258, 2859–2866, 2012.

[37] D. Liu et al., "Hematite Doped Magnetic TiO_2 Nanocomposites with Improved Photocatalytic Activity", Journal: Journal of Alloys and Compounds, 656, 119–126, 2016.

[38] S. Kuang et al., "Fabrication, Characterization and Photoelectrochemical Properties of Fe_2O_3 Modified TiO_2Nanotube Arrays", Journal: Applied Surface Science, 255, 9401–9411, 2009.

[39] T. H. Jeon et al., "Photoelectrochemical and Photocatalytic Behaviors of Hematite-Decorated Titania Nanotube Arrays: Energy Level Mismatch versus Surface Specific Reactivity", Journal: Journal of Physical Chemistry C, 115, 9766–9775, 2011.

[40] H. Dong et al., "An Overview on Limitations of TiO_2-Based Particles for Photocatalytic Degradation of Organic Pollutants and the Corresponding Countermeasures", Journal: Water Research, 70, 77–92, 2015.

[41] K.Senani, "Étude des propriétés photo-électrochimiques des nanofibres de dioxyde de titane décorées par des nanoparticules de l'oxyde de cuivre", Master Thesis, University of August 20th, 1955, Skikda, 2023.

[42] D.Delphine et al., "Small Molecule X-Ray Crystallography, Theory and Workflow, Encyclopedia of Spectroscopy and Spectrometry ", Acadmic press, 2010.

[43] B. Bennstaali, "Méthodes et techniques d'analyse physique", Ed. E.D.I.K, Oran, Algeria, 2003.

[44] R. Bausinger, "Raman Spectroscopy Setup and Experiments for the AdvancedUndergraduate Lab",Education and Training in Optics and Photonics, ISSN 0277-786X, 2015.

[45] A. Belabedii and H. Ghilani, “Green Synthesis of Titanium Dioxide Nanoparticles Using Juniper Extracts and Their Antibacterial Applications”, Master Thesis, University of KasdiMerbah – Ouargla, 2024.

[46] Y.J. Huang et al., “Synthesis and Characterization of Nanosized $MgFe_2O_4$ Powders by Hydrothermal Method”, Journal: Chinese Journal of Inorganic Chemistry, 21, 697–700, 2005.

[47] E. Péré et al., “Quantitative Assessment of Organic Compounds Adsorbed on Silica Gel by FTIR and UV–VIS Spectroscopies: The Contribution of Diffuse Reflectance Spectroscopy”, Journal: Vibrational Spectroscopy, 25, 163–175, 2001.

[48] S. Chaguetmi, “Étude photocatalytique et photoélectrochimique des nanofibres de TiO_2 supportées sur des plaques de titane et sensibilisées par des nanoparticules de ZnS”, PhD Thesis, University of Constantine 1, Algeria, 2014.

[49] A. Naidji and S. Merakchi, “Elaboration et caractérisation des couches minces d’oxyde de cuivre”, Master Thesis, University of Mohamed El Bachir El Ibrahimi – Bordj Bou Arreridj, Algeria, 2021.

[50] M. A. Boda and M. A. Shah, “Enhanced Photo-Electrochemical Potential of Fe_2O_3 Modified TiO_2 Nanotube Array with Multiple Legs”, Journal: Journal of Materials Science: Materials in Electronics, 29, 4641–4651, 2018.

[51] M. Sołtys-Mróz et al., “Band Gap Engineering of Nanotubular Fe_2O_3-TiO_2 Photoanodes by Wet Impregnation”, Journal: Applied Surface Science, 517, 146195, 2020.

[52] A. B. Suriani et al., “Reduced Graphene Oxide–Multiwalled Carbon Nanotubes Hybrid Film with Low Pt Loading as Counter Electrode for Improved Photovoltaic Performance of Dye-Sensitised Solar Cells”, Journal: Journal of Materials Science: Materials in Electronics, 139, 10723–10743, 2017.

[53] M. Sołtys-Mróz et al., “Enhanced Visible Light Photoelectrochemical Water Splitting Using Nanotubular FeOx-TiO_2 Annealed at Different Temperatures”, Journal: Journal of Power Sources, 507, 230274, 2021.

[54] S. Chaguetmi et al., “Visible-Light Photocatalytic Performances of TiO_2 Nanobelts Decorated with Iron Oxide Nanocrystals”, Journal: RSC Advances, 6, 114843–114851, 2016.

[55] P. Luan et al., “Effective Charge Separation in the Rutile TiO_2 Nanorod-Coupled α-Fe_2O_3 with Exceptionally High Visible Activities”, Journal: Scientific Reports, 4, 06180, 2014.

[56] X. Chen et al., “Semiconductor-Based Photocatalytic Hydrogen Generation”, Journal: Chemical Reviews, 110, 6503–6570, 2010.

[57] Y. Hou et al., “Visible Light-Driven α- Fe_2O_3 Nanorod/Graphene/$BiV_{1-x}Mo_xO_4$ Core/Shell Heterojunction Array for Efficient Photoelectrochemical Water Splitting”, Journal: Nano Letters, 12, 6464–6473, 2012.

[58] F. Feng et al., “Boosting hematite photoelectrochemical water splitting by decoration of TiO_2 at the grain boundaries”, Journal: Nano Letters, 368, 959-967, 2019.

[59] A. Othmani et al., “Studies of the Photocatalytic and Electrochemical Performance of the Fe_2O_3/TiO_2 Heteronanostructure”, Journal: Journal of the Iranian Chemical Society, 17, 3339–3349, 2020.

Summary

Abstract

This study focuses on the synthesis, characterization, and photoelectrochemical evaluation of Fe_2O_3-TiO_2 nanotubes (NTs) films for water-splitting applications to produce hydrogen. TiO_2 nanotubes were fabricated using an anodization method, while Fe_2O_3nanoparticles were deposited onto the nanotubes via an impregnation technique. The aim was to develop nanomaterials with controlled crystal size, morphology, and enhanced electronic and optical properties to improve photoelectrochemical performance. Two synthesis strategies were employed: (1) electrochemical anodization at 20 V for 1 hour to produce TiO_2NTs, and (2) impregnation with an iron-containing solution followed by thermal treatment to form Fe_2O_3-TiO_2 hybrid films. The materials were evaluated using a solar simulator and potentiostat to assess their suitability for hydrogen generation through photo-electrolysis.

Keywords:TiO_2NTs, Fe_2O_3 NPs, Fe_2O_3-TiO_2 heterostructures, photosensitization, Photoelectrolysis.

ملخص

هـدف هـذا العملهـو تحضـير، توصـيف وتقيـيم الكهروكيميـائي الضـوئي لأغشـية الأنابيـب النانومترية لـ Fe_2O_3-TiO_2 لتطبيقات تفكيك الماء لإنتـاج الهيـدروجين. حضـرت الأنابيـب النانومترية لـ TiO_2 باستخدام طريقة الأنودة، بينما ترسبت الجسيمات النانومترية لـ Fe_2O_3 على الأنابيب النانوية عبر تقنية الغمر. وكان الهدف من ذلك هو تطوير مـواد نانومتريـة ذات حجم بلوري ومورفولوجيا مضبوطة وخصـائص إلكترونيـة وبصـرية محسّـنة لتحسـين الأداء الكهروكيميائي الضوئي. تم استخدام إستراتيجيتين للتحضير:

(1) الأنودة الكهروكيميائية عند 20 فولت لمدة ساعة واحدة للحصول على أنابيب نانومترية لـ TiO_2، و

(2) الغمـر بمحلـول يحتـوي علـى الحديـد متبوعًـا بالمعالجـة الحراريـة لتشـكيل أغشـية Fe_2O_3-TiO_2الهجينة. تم تقييم المواد باستخدام جهاز محاكاة الطاقة الشمسية ومقياس الجهد لتقييم مدى ملاءمتها لتوليد الهيدروجين من خلال التحليل الكهربائي الضوئي.

الكلمات المفتاحية:الأنابيب النانومترية لـ TiO_2، جسـيمات النانومتريـة لـ Fe_2O_3،أغشـية Fe_2O_3-TiO_2الهجينة، التحسس الضوئي، الكهروكميائية الضوئية.

Résumé

L'objectif de ce travail est la synthèse, la caractérisation et l'évaluation photo électrochimique de film Fe_2O_3-TiO_2 à base de nanotubes (NTs) pour des applications de photoélectrolyse de l'eau afin de produire l'hydrogène. Les nanotubes de TiO_2 ont été préparés par la méthode d'anodisation, tandis que les nanoparticules de Fe_2O_3 ont été déposées par une technique d'imprégnation. L'objectif principal était de développer des nanomatériaux aux propriétés contrôlées, notamment la taille cristalline, la morphologie, ainsi que les caractéristiques électroniques et optiques, afin d'améliorer les performances photoélectrochimiques. Deux approches de synthèse ont été utilisées :
(1) une anodisation électrochimique à 20 V pendant 1 heure pour obtenir des nanotubes de TiO_2, et (2) une imprégnation dans une solution contenant un précurseur de fer suivie d'un traitement thermique pour former des films hybrides Fe_2O_3-TiO_2. Les matériaux obtenus ont été testés à l'aide d'un simulateur solaire et d'un système potentiostatique pour évaluer leur efficacité dans la production d'hydrogène par la photoélectrolyse de l'eau.

Mots-clés:TiO_2NTs, Fe_2O_3NPs, Fe_2O_3-TiO_2 hétérostructures, photosensibilisation, Photoélectrolyse.